INTERNATIONAL JOURNAL FOR NUMERICAL METHODS IN ENGINEERING
Int. J. Numer. Meth. Engng 2005; **62**:870–898
Published online 3 December 2004 in Wiley InterScience (www.interscience.wiley.com). DOI: 10.1002/nme.1194

Charge-induced clustering in multifield particulate flows

T. I. Zohdi*, †

Department of Mechanical Engineering, University of California, 6195 Etcheverry Hall, Berkeley, CA 94720-1740, U.S.A.

SUMMARY

The present work extends recent results in Zohdi (*Int. J. Solids Struct.*, in press; *Proc. Roy. Soc.*, in press) to develop models and robust solution strategies for the direct simulation of the dynamical flow of charged particles undergoing simultaneous contact, surface reactions and heat transfer. Emphasis is placed on the possibility of particle clustering which can lead to the formation of cluster-structures within the particulate flow. A recursive 'staggering' solution scheme is developed, whereby the time-steps are adaptively adjusted to control the rates of convergence within each time-step, and hence, the error associated with the incomplete resolution of the coupled interaction between the various fields and associated constraints. Representative numerical simulations are provided in order to illustrate the character of the model and the solution strategy. Copyright © 2004 John Wiley & Sons, Ltd.

KEY WORDS: charged particulate flows; thermo-chemical coupling; iterative solutions

1. INTRODUCTION

There has been a steady increase in analysis of complex particulate flows, where multifield phenomena, such as electrostatic charging and thermo-chemical coupling, are of interest. Such systems arise in the study of clustering and aggregation of particles in natural science applications where particles collide, cluster, and grow into larger objects. For reviews, see References [1–23]. For general overviews, we refer the reader to Behringer and collaborators: References [24–27]; Hutter and collaborators: References [28–41] and Jaeger and collaborators: References [42–51]. Understanding coupled phenomena in particulate flows is also of interest in modern industrial processes which involve epitaxy, sprays, dust control, etc. For example, in many processes, intentional charging and heating of particulates, such as those in inkjet printers, is critical. Thus, in addition to the calculation of the dynamics of the particles in the particulate flow, the electrostatic and thermo-chemical fields must be determined simultaneously to be able to make accurate predictions of the behaviour of the flow.

*Correspondence to: T. I. Zohdi, Department of Mechanical Engineering, University of California, 6195 Etcheverry Hall, Berkeley, CA 94720-1740, U.S.A.
†E-mail: zohdi@newton.berkeley.edu

Received 6 April 2004
Revised 1 July 2004
Accepted 26 July 2004

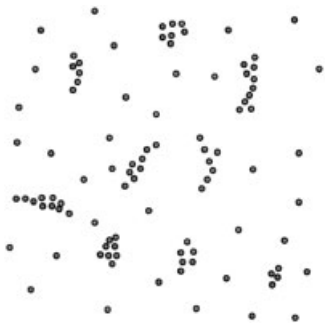

Figure 1. Clustering within a particulate flow.

The present work extends recent results in References [52, 53] to develop models and robust solution strategies to perform direct simulation of the dynamics of particulate media in the presence of multifield effects. In particular, the emphasis placed on developing models and physically-based high-performance solution strategies incorporating near-field interaction between charged particles, interparticulate contact and thermo-chemical coupling due to surface reactions simultaneously, with an eye towards describing particulate clustering (Figure 1).

2. CHARGED INTERACTION BETWEEN PARTICLES

Building on the work found in References [52, 54], we treat the grains as spherical particles, i.e. their rotation with respect to their mass centres is deemed insignificant.[‡] We consider a group of non-intersecting particles (n in total). The equations of motion, for the ith particle in a particulate flow, is

$$m_i \ddot{\boldsymbol{r}}_i = \boldsymbol{\Psi}_i^{\text{tot}}(\boldsymbol{r}_1, \boldsymbol{r}_2, \ldots, \boldsymbol{r}_n) \tag{1}$$

where $\boldsymbol{r}_i$ is the position vector of the ith particle and where $\boldsymbol{\Psi}_i^{\text{tot}}$ represents all forces acting on particle i. In particular, $\boldsymbol{\Psi}_i^{\text{tot}} = \boldsymbol{\Psi}_i^{nf} + \boldsymbol{\Psi}_i^{\text{con}} + \boldsymbol{\Psi}_i^{f\text{ric}}$ represents the forces due to near-field interaction, discussed presently, and normal contact forces and friction, which are discussed afterwards.

2.1. Attraction–repulsion forms

We consider the following relatively general central-force attraction–repulsion form for the near-field forces induced by all particles on particle i

$$\boldsymbol{\Psi}_i^{nf} = \sum_{j \neq i}^{n} \left(\left(\underbrace{\alpha_1 \|\boldsymbol{r}_i - \boldsymbol{r}_j\|^{-\beta_1}}_{\text{attractive part}} - \underbrace{\alpha_2 \|\boldsymbol{r}_i - \boldsymbol{r}_j\|^{-\beta_2}}_{\text{repulsive part}} \right) \underbrace{\boldsymbol{n}_{ij}}_{\text{unit vector}} \right) \tag{2}$$

[‡]Henceforth, we use the term 'grain' and 'particle' interchangeably.

where $\|\cdot\|$ represents the Euclidean norm in R^3, where all of the parameters, α's and β's, are non-negative, and where the normal direction is determined by the difference in the position vectors of their centres, $\boldsymbol{n}_{ij} \stackrel{\text{def}}{=} \boldsymbol{r}_j - \boldsymbol{r}_i / \|\boldsymbol{r}_i - \boldsymbol{r}_j\|$. The force interaction of the form chosen is stable, in the sense that for small disturbances, the system will remain near an equilibrium position, whereas unstable equilibrium will cause the system to move away from an equilibrium position, with an increasing velocity, provided that the exponents are suitably chosen in Equation (2). In order to motivate the concept of stability for such systems we refer to the classical theory of conservative forces. A force field $\boldsymbol{\Psi}^{nf}$ is said to be conservative if and only if there exists a continuously differentiable scalar field V such that $\boldsymbol{\Psi}^{nf} = -\nabla V$. If the force field is conservative, with potential V, then a necessary and sufficient condition for a particle to be in equilibrium at that point is that $\boldsymbol{\Psi}^{nf} = -\nabla V = 0$, in other words $\partial V/\partial x_1 = 0, \partial V/\partial x_2 = 0$ and $\partial V/\partial x_3 = 0$. Forces acting on a particle that are in the direction of a vector connecting the centre of the particle and a point, perhaps the centre of another particle, and whose magnitude depend only on the distance between the particle and the point in question, are called *central forces*. The forces have the following form:

$$\boldsymbol{\Psi}^{nf} = -\mathscr{C}(\|\boldsymbol{r} - \boldsymbol{r}_0\|) \frac{\boldsymbol{r} - \boldsymbol{r}_0}{\|\boldsymbol{r} - \boldsymbol{r}_0\|} = \mathscr{C}(\|\boldsymbol{r} - \boldsymbol{r}_0\|)\boldsymbol{n} \tag{3}$$

where $\boldsymbol{r}$ is the position of the particle, where $\boldsymbol{r}_0$ is the position of the point of attraction/repulsion. The normal direction, connecting the two points, is given by $\boldsymbol{n} = \boldsymbol{r}_0 - \boldsymbol{r}/\|\boldsymbol{r} - \boldsymbol{r}_0\|$. The central force is one of attraction if $\mathscr{C}(\|\boldsymbol{r} - \boldsymbol{r}_0\|) > 0$ and one of repulsion if $\mathscr{C}(\|\boldsymbol{r} - \boldsymbol{r}_0\|) < 0$. We remark that a central force field is always conservative, since $\nabla \times \boldsymbol{\Psi}^{nf} = \boldsymbol{0}$. For example, consider $V = (\alpha_1 \|\boldsymbol{r} - \boldsymbol{r}_0\|^{-\beta_1+1})/ - \beta_1 + 1 - [(\alpha_2 \|\boldsymbol{r} - \boldsymbol{r}_0\|^{-\beta_2+1})/ - \beta_2 + 1]$, where all of the parameters, α's and β's, are non-negative. The gradient yields $-\nabla V = \boldsymbol{\Psi}^{nf} = (\alpha_1 \|\boldsymbol{r} - \boldsymbol{r}_0\|^{-\beta_1} - \alpha_2 \|\boldsymbol{r} - \boldsymbol{r}_0\|^{-\beta_2})\boldsymbol{n}$, which is the form introduced previously. If a particle which is displaced slightly from an equilibrium point tends to return to that point, then we call that point a point of stability or stable point and the equilibrium is said to be stable. Otherwise, we say that the point is one of instability and the equilibrium is unstable. *A necessary and sufficient condition that an equilibrium point be one of stability is that the potential V at the point be a minimum*. The general condition by which a potential is stable for the multidimensional case can be determined by studying the properties of the Hessian,

$$[\mathbb{H}] \stackrel{\text{def}}{=} \begin{bmatrix} \dfrac{\partial^2 V}{\partial x_1 \partial x_1} & \dfrac{\partial^2 V}{\partial x_1 \partial x_2} & \dfrac{\partial^2 V}{\partial x_1 \partial x_3} \\ \dfrac{\partial^2 V}{\partial x_2 \partial x_1} & \dfrac{\partial^2 V}{\partial x_2 \partial x_2} & \dfrac{\partial^2 V}{\partial x_2 \partial x_3} \\ \dfrac{\partial^2 V}{\partial x_3 \partial x_1} & \dfrac{\partial^2 V}{\partial x_3 \partial x_2} & \dfrac{\partial^2 V}{\partial x_3 \partial x_3} \end{bmatrix} \tag{4}$$

around an equilibrium point. A sufficient condition for V to attain a minimum at an equilibrium point is that the Hessian be positive definite (which implies that V is locally convex). For more details see Reference [55]. The central force potential chosen in this work is *near-field* stable for motion in the normal direction, i.e. the line connecting the centres of the particles. For disturbances in directions orthogonal to the normal direction, the potential is neutrally stable, i.e. the Hessian's determinant is zero, thus indicating that the potential does not change for such

perturbations. Thus, in order to determine stable parameter combinations, consider a potential function for a single particle, in one-dimensional motion, representing the motion in the normal direction, attracted and repulsed from a point r_0 measured by the co-ordinate r,

$$V = \frac{\alpha_1}{-\beta_1 + 1}|r - r_0|^{-\beta_1+1} - \frac{\alpha_2}{-\beta_2 + 1}|r - r_0|^{-\beta_2+1} \tag{5}$$

whose derivative produces the form of interaction forces introduced earlier:

$$\Psi^{nf} = -\frac{\partial V}{\partial r} = (\alpha_1|r - r_0|^{-\beta_1} - \alpha_2|r - r_0|^{-\beta_2})n \tag{6}$$

where $n = r_0 - r/|r - r_0|$. We remark that the motion in the normal direction is relevant for central forces of this type. For stability, we require

$$\frac{\partial^2 V}{\partial r^2} = -\alpha_1\beta_1|r - r_0|^{-\beta_1-1} + \alpha_2\beta_2|r - r_0|^{-\beta_2-1} > 0 \tag{7}$$

A static equilibrium point, $r = r_e$, can be calculated from $\Psi^{nf}(|r_e - r_0|) = -\alpha_1|r_e - r_0|^{-\beta_1} + \alpha_2|r_e - r_0|^{-\beta_2} = 0$, which implies

$$|r_e - r_0| = \left(\frac{\alpha_2}{\alpha_1}\right)^{1/(-\beta_1+\beta_2)} \tag{8}$$

Inserting Equation (8) into Equation (7) yields a restriction for stability, $\beta_2/\beta_1 > 1$.

One can consider the convexity requirement on the potential to insure that the perturbed motion to a dynamical state remain small. Consider the dynamics of a particle in the normal direction, with a perturbation, $\tilde{r} = r + \delta r, m\ddot{\tilde{r}} = \Psi^{nf}(\tilde{r})$, where r is the perturbation-free position vector of the particle, governed by $m\ddot{r} = \Psi^{nf}(r)$. Taking the difference between these two differential equations yields

$$m\ddot{\delta}r = \Psi^{nf}(\tilde{r}) - \Psi^{nf}(r) \approx \left.\frac{\partial\Psi^{nf}}{\partial r}\right|_{\tilde{r}=r} \delta r + \cdots \Rightarrow m\ddot{\delta}r - \left.\frac{\partial\Psi^{nf}}{\partial r}\right|_{\tilde{r}=r} \delta r \approx 0 \tag{9}$$

If $\partial\Psi^{nf}(r)/\partial r$ is positive, there will be exponential growth of the perturbation, while if $\partial\Psi^{nf}(r)/\partial r$ is negative, there will be oscillatory behaviour of the perturbation. Thus, since $-\partial^2 V/\partial r^2 = \partial\Psi^{nf}/\partial r$, we have

$$m\ddot{\delta}r + \left.\frac{\partial^2 V}{\partial r^2}\right|_{\tilde{r}=r} \delta r \approx 0 \tag{10}$$

The convexity of the potential simply corresponds to the positiveness of the stiffness at r. In addition to the instabilities about an equilibrium point, the point at which the potential changes from a convex to concave character is a source of long-range instability (Figure 2). For motion in the normal direction, we have

$$\frac{\partial^2 V}{\partial r^2} = -\beta_1\alpha_1|r - r_0|^{-\beta_1-1} + \beta_2\alpha_2|r - r_0|^{-\beta_2-1} = 0 \tag{11}$$

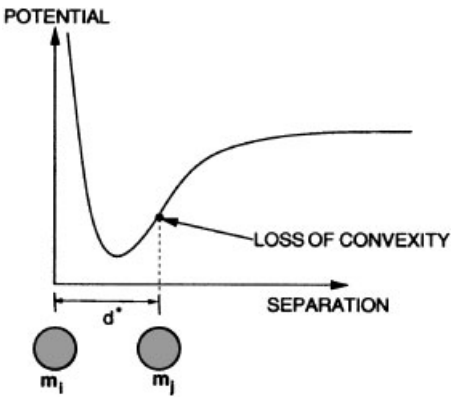

Figure 2. Identification of an inflection point (loss of convexity).

thus leading to

$$|r - r_0| = \left(\frac{\beta_2 \alpha_2}{\beta_1 \alpha_1}\right)^{1/(-\beta_1+\beta_2)} = d^* \tag{12}$$

Thus, the preceding analysis indicates that, for the three-dimensional case, the interaction should be cut-off beyond $\|\boldsymbol{r}_i - \boldsymbol{r}_j\| = d^*$ to avoid long-range (central-force) instabilities.

2.2. *Clustering via binding forces*

In many applications the near-fields can dramatically change when the particles are very close to one another, leading to increased repulsion or attraction. Of specific interest in this work is interparticle binding leading to clustering[§] (Figure 1). A particularly easy way to model this is via an activation of a near-field attractive augmentation of the form, if $\|\boldsymbol{r}_i - \boldsymbol{r}_j\| \leqslant (b_i + b_j)\delta_{\mathrm{a}}$

$$\boldsymbol{\Psi}_i^{nf,a} \stackrel{\text{def}}{=} \boldsymbol{\Psi}_i^{nf} + \underbrace{\alpha_{\mathrm{a}} \|\boldsymbol{r}_i - \boldsymbol{r}_j\|^{-\beta_{\mathrm{a}}}}_{\boldsymbol{\Psi}^a \stackrel{\text{def}}{=} \text{BINDING FORCE}} \tag{13}$$

where b_i and b_j are the radii of the particles,[¶] and where $1 \leqslant \delta_{\mathrm{a}}$ is the critical distance needed for the augmentation to become active. The corresponding binding potential is (active, if $\|\boldsymbol{r}_i - \boldsymbol{r}_j\| \leqslant (b_i + b_j)\delta_{\mathrm{a}}$)

$$V_{\mathrm{a}}(\|\boldsymbol{r}_i - \boldsymbol{r}_j\|) = \frac{\alpha_{\mathrm{a}} \|\boldsymbol{r}_i - \boldsymbol{r}_j\|^{-\beta_{\mathrm{a}}+1}}{-\beta_{\mathrm{a}} + 1} \tag{14}$$

[§]Sometimes the term 'agglomeration' is used in the literature.
[¶]They will be taken to be the same, later in the simulations.

Denoting the nominal (unclustered) equilibrium distance by d_e and the equilibrium distance, when clustering is active, by d_a, we have, with $\beta_a = \beta_1$

$$\|\boldsymbol{r}_i - \boldsymbol{r}_j\| = \left(\frac{\alpha_2}{\alpha_1 + \alpha_a}\right)^{1/(-\beta_1+\beta_2)} = d_a \leqslant d_e = \left(\frac{\alpha_2}{\alpha_1}\right)^{1/(-\beta_1+\beta_2)} \tag{15}$$

Clearly, with such a model, the magnitude of α_a must be limited so that no inter-penetration of the particles are possible, i.e. $\|\boldsymbol{r}_i - \boldsymbol{r}_j\| \geqslant b_i + b_j$.

Remark 1
For many engineering materials, some surface adhesion persists, which can lead to a sticking phenomena between surfaces, even when no explicit charging has occurred. For more details, see Reference [56].

Remark 2
There are similarities between particulate flow models and those found in the field of molecular dynamics (MD), where the motion of individual atoms is described by the Newton's second law with the forces computed from a prescribed potential energy function, $V(\boldsymbol{r}), m\ddot{\boldsymbol{r}} = -\nabla V(\boldsymbol{r})$. For reviews of MD, see References [57–60]. More complex (tertiary and binary) potential are possible, and take the form of familiar Mie, Lennard-Jones, and Morse potentials [61]. The expansions beyond the binary interactions introduce either three-body terms directly [62] or as modification of the two-body representations [63]. For reviews, we refer the reader to Reference [64].

Remark 3
Depending on the degree of near-field strength, the particulate system can exhibit vibratory motion. This can be qualitatively explained by recognizing that the governing equations are formally similar to classical second order equations describing harmonic oscillators. For more details, see Reference [52].

3. IMPACT AND MOMENTUM TRANSFER

Following Zohdi [52], cases where mechanical contact occurs between particles, in the presence of near-field interaction forces, which can be quite strong, and comparable in magnitude to the contact forces, are now considered. We assume that the particles remain spherical after impact, i.e. any permanent deformation is negligible. Also, in contrast with the usual analyses of impacting particles, which neglect all other forces except those of mechanical contact, we include the near-field effects.[‖]

3.1. Normal contact

For two impacting particles i and j, normal to the line of impact, a statement for a balance of linear momentum relating the states before impact (time $= t$) and after impact (time $= t + \delta t$)

[‖]Due to the non-standard analysis found inthis section, we concisely re-iterate parts of an analysis found in press in Reference [52].

reads as

$$m_i v_{in}(t) + m_j v_{jn}(t) + \int_t^{t+\delta t} \boldsymbol{E}_i \cdot \boldsymbol{n}_{ij}\, \mathrm{d}t + \int_t^{t+\delta t} \boldsymbol{E}_j \cdot \boldsymbol{n}_{ij}\, \mathrm{d}t$$

$$= m_i v_{in}(t+\delta t) + m_j v_{jn}(t+\delta t) \tag{16}$$

where the subscript n denotes the normal component of the velocity (along the line connecting particle centres) and the $\boldsymbol{E}$'s represent all forces induced by near-field interaction with other particles, as well as all other external forces, if any, to the pair. If one isolates one of the members of the colliding pair, then

$$m_i v_{in}(t) + \int_t^{t+\delta t} I_n\, \mathrm{d}t + \int_t^{t+\delta t} \boldsymbol{E}_i \cdot \boldsymbol{n}_{ij}\, \mathrm{d}t = m_i v_{in}(t+\delta t) \tag{17}$$

where $\int_t^{t+\delta t} I_n\, \mathrm{d}t$ is the total normal impulse due to impact. For a pair of particles undergoing impact, let us consider a decomposition of the collision event into a compression (δt_1) and recovery (δt_2) phase, i.e. $\delta t = \delta t_1 + \delta t_2$. Between the compression and recovery phases, the particles achieve a common velocity, denoted v_{cn}, at the intermediate time $t + \delta t_1$. A common normal velocity for particles should be interpreted as indicating that the relative velocity in the normal direction between particle centres is zero. We may write for particle i, along the normal, in the compression phase of impact

$$m_i v_{in}(t) + \int_t^{t+\delta t_1} I_n\, \mathrm{d}t + \int_t^{t+\delta t_1} \boldsymbol{E}_i \cdot \boldsymbol{n}_{ij}\, \mathrm{d}t = m_i v_{cn} \tag{18}$$

and in the recovery phase

$$m_i v_{cn} + \int_{t+\delta t_1}^{t+\delta t} I_n\, \mathrm{d}t + \int_{t+\delta t_1}^{t+\delta t} \boldsymbol{E}_i \cdot \boldsymbol{n}_{ij}\, \mathrm{d}t = m_i v_{in}(t+\delta t) \tag{19}$$

For the other particle (j), in the compression phase,

$$m_j v_{jn}(t) - \int_t^{t+\delta t} I_n\, \mathrm{d}t + \int_t^{t+\delta t_1} \boldsymbol{E}_j \cdot \boldsymbol{n}_{ij}\, \mathrm{d}t = m_j v_{cn} \tag{20}$$

and in the recovery phase

$$m_j v_{cn} - \int_{t+\delta t_1}^{t+\delta t} I_n\, \mathrm{d}t + \int_{t+\delta t_1}^{t+\delta t} \boldsymbol{E}_j \cdot \boldsymbol{n}_{ij}\, \mathrm{d}t = m_j v_{jn}(t+\delta t) \tag{21}$$

This leads to an expression for the coefficient of restitution

$$e \stackrel{\text{def}}{=} \frac{\displaystyle\int_{t+\delta t_1}^{t+\delta t} I_n \,\mathrm{d}t}{\displaystyle\int_{t}^{t+\delta t_1} I_n \,\mathrm{d}t} = \frac{m_i(v_{in}(t+\delta t) - v_{cn}) - E_{in}(t+\delta t_1, t+\delta t)}{m_i(v_{cn} - v_{in}(t)) - E_{in}(t, t+\delta t_1)}$$

$$= \frac{-m_j(v_{jn}(t+\delta t) - v_{cn}) + E_{jn}(t+\delta t_1, t+\delta t)}{-m_j(v_{cn} - v_{jn}(t)) + E_{jn}(t, t+\delta t_1)} \tag{22}$$

where

$$E_{in}(t+\delta t_1, t+\delta t_2) \stackrel{\text{def}}{=} \int_{t+\delta t_1}^{t+\delta t} \boldsymbol{E}_i \cdot \boldsymbol{n}_{ij} \,\mathrm{d}t, \quad E_{jn}(t+\delta t_1, t+\delta t_2) \stackrel{\text{def}}{=} \int_{t+\delta t_1}^{t+\delta t} \boldsymbol{E}_j \cdot \boldsymbol{n}_{ij} \,\mathrm{d}t$$
$$E_{in}(t, t+\delta t_1) \stackrel{\text{def}}{=} \int_{t}^{t+\delta t_1} \boldsymbol{E}_i \cdot \boldsymbol{n}_{ij} \,\mathrm{d}t, \quad E_{jn}(t, t+\delta t_1) \stackrel{\text{def}}{=} \int_{t}^{t+\delta t_1} \boldsymbol{E}_j \cdot \boldsymbol{n}_{ij} \,\mathrm{d}t \tag{23}$$

If we eliminate v_{cn}, we obtain an expression for e

$$e = \frac{v_{jn}(t+\delta t) - v_{in}(t+\delta t) + D_{ij}(t+\delta t_1, t+\delta t)}{v_{in}(t) - v_{jn}(t) + D_{ij}(t, t+\delta t_1)} \tag{24}$$

where we define the operator over any time interval (a, b) as $D_{ij}(a,b) \stackrel{\text{def}}{=} (1/m_i)E_{in}(a,b) - (1/m_j)E_{jn}(a,b)$. Thus, we may rewrite Equation (24) as

$$v_{jn}(t+\delta t) = v_{in}(t+\delta t) - D_{ij}(t+\delta t_1, t+\delta t) + e(v_{in}(t) - v_{jn}(t) + D_{ij}(t, t+\delta t_1)) \tag{25}$$

It is convenient to denote the average force acting on the particle from external sources as $\bar{E}_{in} \stackrel{\text{def}}{=} \frac{1}{\delta t}\int_t^{t+\delta t} \boldsymbol{E}_i \cdot \boldsymbol{n}_{ij} \,\mathrm{d}t$. If e is explicitly known, then one can write, combining Equations (24) and (25)

$$v_{in}(t+\delta t) = \frac{m_i v_{in}(t) + m_j(v_{jn}(t) - e(v_{in}(t) - v_{jn}(t)))}{m_i + m_j}$$
$$+ \frac{(\bar{E}_{in} + \bar{E}_{jn})\delta t - m_j(eD_{ij}(t, t+\delta t_1) - D_{ij}(t+\delta t_1, t+\delta t))}{m_i + m_j} \tag{26}$$

where, once $v_{in}(t+\delta t)$ is known, one can subsequently also solve for $v_{jn}(t+\delta t)$ via Equation (25).

Remark 1

Clearly, the forces needed to compute terms in coefficient of restitution e, such as E_{in}, E_{jn} and D_{ij} depend on the particle kinetics during impact, i.e. the outcome of the system dynamics, and thus implicitly on e. In other words, an implicit system of non-linear coupled equations arises. In order to solve the system of coupled non-linear equations, later in this work, an iterative (fixed-point type) staggering process is developed.

Remark 2
Equation (24) collapses to the classical expression for the ratio of the relative velocities before and after impact, if the near-field forces are negligible,

$$e \overset{\text{def}}{=} \frac{v_{jn}(t+\delta t) - v_{in}(t+\delta t)}{v_{in}(t) - v_{jn}(t)} \tag{27}$$

Later, it will be useful to define the average impulsive normal contact force between the particles acting during the impact event as

$$\bar{I}_n \overset{\text{def}}{=} \frac{1}{\delta t}\int_t^{t+\delta t} I_n \,\mathrm{d}t = \frac{m_i(v_{in}(t+\delta t) - v_{in}(t))}{\delta t} - \bar{E}_{in} \tag{28}$$

In particular, as will be done later in the analysis, when we discretize the equations of motion with a discrete (finite difference) time-step of Δt, where $\delta t \ll \Delta t$, we shall define the impulsive normal contact contribution to the total force (Equation (1)) to be

$$\boldsymbol{\Psi}^{\text{con}} = \frac{\bar{I}_n \delta t}{\Delta t}\boldsymbol{n}_{ij} \tag{29}$$

which will be included in the total force acting on a particle, $\boldsymbol{\Psi}_i^{\text{tot}} = \boldsymbol{\Psi}_i^{nf,a} + \boldsymbol{\Psi}_i^{\text{con}} + \boldsymbol{\Psi}_i^{\text{fric}}$. Furthermore, at the implementation level, we choose $\delta t = \gamma \Delta t$, where $0 < \gamma \ll 1$ and where Δt is the time-step discretization size, which will be introduced later in the work.** We assume $\delta t_1 + \delta t_2 = \delta t_1 + e\delta t_1$, which immediately allows the following definitions:

$$\delta t_1 = \frac{\gamma \Delta t}{1+e} \quad \text{and} \quad \delta t_2 = \frac{e\gamma \Delta t}{1+e} \tag{30}$$

These results are consistent with the fact that the recovery time vanishes (all compression and no recovery) for $e \to 0$ (asymptotically plastic) and, as $e \to 1$, the recovery time equal the compression time ($\delta t_2 = \delta t_1$, asymptotically elastic). For a more detailed treatment of impact duration times, see Reference [65].

3.2. Friction

To account for frictional stick-slip phenomena, during impact for an arbitrary particle pair (i and j), the tangential velocities at the beginning of the impact time interval, time $= t$, are computed by subtracting the relative normal velocity away from the total relative velocity,

$$\boldsymbol{v}_{jt}(t) - \boldsymbol{v}_{it}(t) = (\boldsymbol{v}_j(t) - \boldsymbol{v}_i(t)) - ((\boldsymbol{v}_j(t) - \boldsymbol{v}_i(t)) \cdot \boldsymbol{n}_{ij})\boldsymbol{n}_{ij} \tag{31}$$

One then writes the equation for tangential momentum change during impact for the ith particle $m_i v_{it}(t) - \bar{I}_f \delta t + \bar{E}_{it}\delta t = m_i v_{ct}$, where the friction contribution is $\bar{I}_f = \frac{1}{\delta t}\int_t^{t+\delta t} I_f \,\mathrm{d}t$, where the total contributions from all other particles in the tangential direction ($\boldsymbol{t}$) are $\bar{E}_{it} = \frac{1}{\delta t}\int_t^{t+\delta t} \boldsymbol{E}_i \cdot \boldsymbol{t}\,\mathrm{d}t$ and where v_{ct} is the common tangential velocity of particles i and j in the tangential direction.†† Similarly, for the jth particle we have $m_j v_{jt}(t) + \bar{I}_f \delta t + \bar{E}_{jt}\delta t = m_j v_{ct}$.

**A typical choice is $0 < \gamma \leqslant 0.01$. The system is insensitive to γ below 0.01.
††They do not move relative to one another.

There are two unknowns, $\bar{I}_f$ and v_{ct}. The main quantity of interest is $\bar{I}_f$, which can be solved for

$$\bar{I}_f = \frac{(m_j \bar{E}_{it} - m_i \bar{E}_{jt})\delta t + m_i m_j (v_{it}(t) - v_{jt}(t))}{(m_i + m_j)\delta t} \tag{32}$$

The friction force is then $\boldsymbol{\Psi}_i^{f\,\mathrm{ric}} = |\bar{I}_f|\boldsymbol{t}$. However, consistent with stick-slip models of Coloumb friction, one first assumes no slip occurs. If $|\bar{I}_f| > \mu_s|\bar{I}_n|$, where μ_s is the coefficient of *static* friction, then slip must occur and a dynamic sliding friction model is used. If sliding occurs, the friction force is assumed to be proportional to the normal force and opposite to the direction of relative tangent motion, i.e.

$$\boldsymbol{\Psi}_i^{f\,\mathrm{ric}} \stackrel{\mathrm{def}}{=} \mu_d \|\boldsymbol{\Psi}^{\mathrm{con}}\| \frac{\boldsymbol{v}_{jt} - \boldsymbol{v}_{it}}{\|\boldsymbol{v}_{jt} - \boldsymbol{v}_{it}\|} = -\boldsymbol{\Psi}_j^{f\,\mathrm{ric}} \tag{33}$$

where μ_d the dynamic coefficient of friction and where $\mu_d \leqslant \mu_s$. There are limitations on the friction coefficients for such models to make physical sense. For general dynamic analyses of such mechanical models involving friction see References [66–70]. For a recent overview, see Reference [71].

4. THERMO-CHEMICAL COUPLING

It is important to realize that, in reality, the phenomenological parameter e depends on the severity of the impact velocity. For extensive experimental data, see Reference [72]. Qualitatively, the coefficient of restitution will decrease with the relative velocity of approach. A mathematical idealization of the behaviour can be constructed as follows:

$$e \stackrel{\mathrm{def}}{=} \max\left(e_0\left(1 - \frac{\Delta v_n}{v^*}\right), e^-\right) \tag{34}$$

where v^* is a critical threshold velocity (normalization) parameter and where the relative velocity of approach is defined by $\Delta v_n \stackrel{\mathrm{def}}{=} |v_{jn}(t) - v_{in}(t)|$ and e^- is a (typically small) lower limit to the coefficient of restitution.[‡‡] In certain applications, in addition to the near-field and contact effects introduced thus far, thermal behaviour is of interest. For example, applications arise in the study of interstellar particulate dust flows in the presence of dilute hydrogen-rich gas. In many cases, the generation of heat in such flows can be traced to the reactivity of the contacting particle surfaces. Subsequent thermal effects can strongly affect the mechanics of impact, for example, due to thermal softening. For instance, the presence of a reactive substance (gas) adsorbed onto the surface of interplanetary dust can be a source of intense heat generation, through thermochemical reactions activated by impact forces, which thermally softens the material, thus reducing the coefficient of restitution, which in turn strongly affects the mechanical impact event itself (Figure 3).

[‡‡]Lower values of v^* represent softer materials, which exhibit more dissipation upon impact than harder materials.

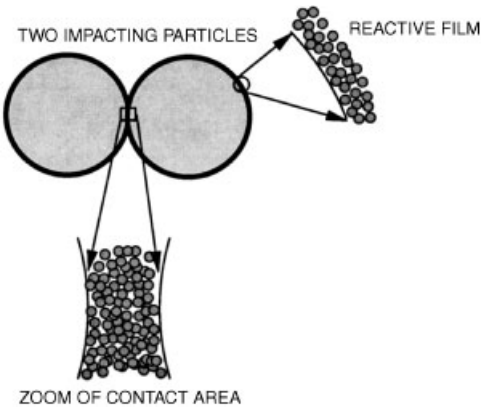

Figure 3. Presence of dilute (smaller-scale) reactive gas particles adsorbed onto the surface of two impacting particles.

A somewhat *ad hoc* approach, building on the relation in Equation (34), is to construct a thermally dependent coefficient of restitution as follows:

$$e \stackrel{\text{def}}{=} \left(\max\left(e_0\left(1-\frac{\Delta v_n}{v^*}\right), e^-\right)\right)\left(\max\left(\left(1-\frac{\theta}{\theta^*}\right), 0\right)\right) \tag{35}$$

where θ^* can be considered as a thermal softening temperature.[§§] In order to determine the thermal state of the particles, we shall decompose the heat generation and transfer processes into two stages. Stage I describes the extremely short time interval when impact occurs, $\delta t \ll \Delta t$, and accounts for the effects of chemical reactions, which are relevant in certain applications, and energy release due to mechanical straining. Stage II accounts for the post impact behaviour involving convective and radiative effects.

4.1. Stage I: impact

Throughout the analysis, we shall use the most simplified models possible. Consistent with the particle-based philosophy, it is assumed that the temperature fields are uniform in the particles.[¶¶] We consider an energy balance, governing the inter-conversions of mechanical, thermal and chemical energy in a system, dictated by the first law of thermodynamics. Accordingly, we require the time rate of change of the sum of the kinetic energy ($\mathscr{K}$) and stored energy ($\mathscr{S}$) to be equal to the work rate (power, $\mathscr{P}$) and the net heat supplied ($\mathscr{H}$)

$$\frac{\mathrm{d}}{\mathrm{d}t}(\mathscr{K}+\mathscr{S}) = \mathscr{P}+\mathscr{H} \tag{36}$$

[§§]Lower values of θ^* represent more thermally sensitive materials, with relatively more dissipative impact events. Generally, decreasing v^* and θ^* makes the system more dissipative and, consequently, easier to simulate, since it is less stiff.

[¶¶]Thus, the gradient of the temperature within the particle is zero, i.e. $\nabla\theta = \mathbf{0}$. Thus, a Fourier-type law for the heat flux will register a zero value, $\boldsymbol{q} = -\mathbb{K}\cdot\nabla\theta = \mathbf{0}$.

where the stored energy is comprised of a thermal part, $\mathscr{S}(t) = mC\theta(t)$, where C is the heat capacity per unit mass, and, consistent with our assumptions that the particles deform negligibly during impact, *a negligible mechanical stored energy part*. The kinetic energy is $\mathscr{K}(t) = \frac{1}{2} m\boldsymbol{v}(t) \cdot \boldsymbol{v}(t)$. The mechanical power term is due to the forces acting on a particle

$$\mathscr{P} = \frac{\mathrm{d}\mathscr{W}}{\mathrm{d}t} = \boldsymbol{\Psi}^{\mathrm{tot}} \cdot \boldsymbol{v} \tag{37}$$

and, because $\frac{\mathrm{d}\mathscr{K}}{\mathrm{d}t} = m\dot{\boldsymbol{v}} \cdot \boldsymbol{v}(t)$, and a balance of momentum $m\dot{\boldsymbol{v}} \cdot \boldsymbol{v} = \boldsymbol{\Psi}^{\mathrm{tot}} \cdot \boldsymbol{v}$ and thus $\frac{\mathrm{d}\mathscr{K}}{\mathrm{d}t} = \frac{\mathrm{d}\mathscr{W}}{\mathrm{d}t} = \mathscr{P}$, leading to $\frac{\mathrm{d}\mathscr{S}}{\mathrm{d}t} = \mathscr{H}$. The primary source of heat is due to chemical reactions, where the reactive layer generates heat upon impact. The chemical reaction energy is defined as $\delta\mathscr{H} \stackrel{\mathrm{def}}{=} \int_t^{t+\delta t} \mathscr{H}\,\mathrm{d}t$. Equation (36) can be rewritten for the temperature at time $= t + \delta t$ as

$$\theta(t + \delta t) = \theta(t) + \frac{\delta\mathscr{H}}{mC} \tag{38}$$

The energy released from the reactions are assumed to be proportional to the amount of the gaseous substance available to be compressed in the contact area between the particles. A typical, *ad hoc* approximation in combustion processes is to write, for example, a linear relation

$$\delta\mathscr{H} \approx \kappa \min\left(\frac{|\bar{I}_n|}{I_n^*},\ 1\right)\pi b^2 \tag{39}$$

where κ is a reaction constant, energy per unit area, I_n^* is normalization parameter and b is the particle radius. For details, see Reference [73], for example. For the grain sizes and material properties of interest, the term, $\delta\mathscr{H}/mC$, in Equation (38) indicates that values of κ of approximately $\kappa \approx 10^6\,\mathrm{J/m^2}$ will generate significant amounts of heat.[‖‖] *Clearly, these equations are coupled to those of impact through the coefficient of restitution and the velocity-dependent impulses*. Additionally, the post-collision velocities are computed from the momentum relations which are coupled to the temperature. Later in the analysis, this equation is incorporated into an overall staggered fixed-point iteration scheme, whereby the temperature is predicted for a given velocity field, and then the velocities are recomputed with the new temperature field, etc. The process is repeated until the fields change negligibly between successive iterations. The entire set of equations are embedded within a larger overall set of equations later in the analysis, and solved in a recursively staggered manner. A detailed numerical analysis of multifield contact between bodies using a continuum description is beyond the scope of the present work. However, such analyses can be found in Reference [71].

4.2. Stage II: post-impact

After impact, it is assumed that a process of convection, for example governed by Newton's law of cooling, and radiation according to a simple Stefan–Boltzmann law transpires. As before, it is assumed that the temperature fields are uniform within the particles, thus conduction within the particles is negligible. We remark that the validity of using a lumped thermal model, i.e.

[‖‖] By construction, this model has increased heat production, via $\delta\mathscr{H}$, for increasing κ.

ignoring temperature gradients and assuming a uniform temperature within a particle, is dictated by the magnitude of the Biot number. A small Biot number indicates that such an approximation is reasonable. The Biot number for spheres scales with the ratio of particle volume (V) to particle surface area (a_s), $V/a_s = b/3$, which indicates that a uniform temperature distribution is appropriate, since the particles, by definition, are small. We also assume that the dynamics of the (dilute) gas does not affect the motion of the (much heavier) particles. The gas only supplies a reactive thin film on the particles' surfaces. The first law reads

$$\frac{\mathrm{d}(K+U)}{\mathrm{d}t} = m\dot{\boldsymbol{v}}\cdot\boldsymbol{v} + mC\dot{\theta} = \underbrace{\boldsymbol{\Psi}^{\mathrm{tot}}\cdot\boldsymbol{v}}_{\text{mechanical power}} - \underbrace{h_c a_s(\theta-\theta_0)}_{\text{convective heating}} - \underbrace{\mathscr{B}a_s\varepsilon(\theta^4-\theta_s^4)}_{\text{far-field radiation}} \tag{40}$$

where θ_0 is the temperature of the ambient gas, where θ_s is the temperature of the far field surface (for example a container surrounding the flow) with which radiative exchange is made, $\mathscr{B} = 5.67\times10^{-8}W/(m^2-K)$ is the Stefan–Boltzmann constant, where $0\leqslant\varepsilon\leqslant1$ is the emissivity, which indicates how efficiently the surface radiates energy compared to a black-body (an ideal emitter), where $0\leqslant h_c$ is the heating due to convection (Newton's law of cooling) into the dilute gas and where a_s is the surface area of a particle. It is assumed that the radiation exchange between the particles is negligible.*** For the applications considered, typically, h_c is quite small, and play a small role in the heat transfer processes.††† From a balance of momentum we have $m\dot{\boldsymbol{v}}\cdot\boldsymbol{v} = \boldsymbol{\Psi}^{\mathrm{tot}}\cdot\boldsymbol{v}$ and Equation (40) becomes

$$mC\dot{\theta} = -h_c a_s(\theta-\theta_0) - \mathscr{B}a_s\varepsilon(\theta^4-\theta_s^4) \tag{41}$$

Therefore, after temporal integration with the previously used finite difference time-step of $\Delta t \gg \delta t$, implying, $\theta(t) = \theta(t+\delta t)$, where $\theta(t+\delta t)$ is computed from Equation (38), and we have

$$\theta(t+\Delta t) = \frac{mC}{mC+h_c a_s\Delta t}\,\theta(t) - \frac{\Delta t\mathscr{B}a_s\varepsilon}{mC+h_c a_s\Delta t}\,(\theta^4(t+\Delta t)-\theta_s^4) + \frac{h_c a_s\Delta t\theta_0}{mC+h_c a_s\Delta t} \tag{42}$$

This implicit non-linear equation for θ, *far each particle*, is added into the fixed-point scheme with the equations of momentum balance, and solved simultaneously with a *multifield* staggering scheme, which we now discuss.

Remarks

Convection heat transfer is comprised of two primary mechanisms, one due to primarily random molecular motion (diffusion) and the other by bulk motion of a fluid, in our case a gas, surrounding the particles. As we have indicated, in the applications of interest here, the gas is dilute and the Reynold's number is small, thus convection plays a very small role in the heat transfer process. We recall that a blackbody is an ideal radiating surface having the following

***Various arguments for such an assumption can be found in the classical text of Bohren and Huffman [74].

†††The Reynold's number, which measures the ratio of the inertial forces to viscous forces in the surrounding gas, and dictates the magnitude of these parameters, is extremely small in the regimes considered.

properties:

- A blackbody absorbs all incident radiation, regardless of wavelength and direction,
- For a prescribed temperature and wavelength, no surface can emit more energy than a blackbody and
- Although the radiation emitted by a blackbody is a function of wavelength and temperature, it is independent of direction.

Since a blackbody is a perfect emitter, it serves as a standard against which the radiative properties of actual surfaces may be compared. The Stefan–Boltzmann law, which is computed by integrating the Planck representation of the emissive power distribution of a blackbody over all wavelengths,[‡‡‡] allows the calculation of the amount of radiation emitted in all directions and over all wavelengths simply from the knowledge of the temperature of the blackbody.

5. AN STAGGERED/INTERNALLY-ITERATIVE SOLUTION SCHEME

We now develop a staggering scheme by extending an approach found in References [52–54, 75, 76]. Broadly speaking, staggering schemes proceed by solving each field equation individually, allowing only the primary field variable to be active. After the solution of each field equation, the primary field variable is updated, and the next field equation is addressed in a similar manner. Such approaches have a long history in the computational mechanics community. For example, see References [77–85].

We consider an abstract setting, whereby one solves for the particle positions, assuming the thermal fields fixed,

$$\mathscr{A}_1(\underline{\boldsymbol{r}^{L+1,K+1}}, \theta^{L+1,K}) = \mathscr{F}_1(\boldsymbol{r}^{L+1,K}, \theta^{L+1,K}) \tag{43}$$

then one solves for the thermal fields, assuming the particle positions fixed,

$$\mathscr{A}_2(\boldsymbol{r}^{L+1,K+1}, \underline{\theta^{L+1,K+1}}) = \mathscr{F}_2(\boldsymbol{r}^{L+1,K+1}, \theta^{L+1,K}) \tag{44}$$

where only the underlined variable is 'active', where L indicates the time-step and where K indicates the iteration counter. Within the staggering scheme, implicit time-stepping methods, with time-step size adaptivity, will be used throughout the upcoming analysis. We start by treating the equations of motion for the particles.

Accordingly, after time discretization of the acceleration term in the equations of motion (Equation (1)) for a particle

$$\ddot{\boldsymbol{r}}_i^{L+1} \approx \frac{\boldsymbol{r}_i^{L+1} - 2\boldsymbol{r}_i^{L} + \boldsymbol{r}_i^{L-1}}{(\Delta t)^2} \tag{45}$$

[‡‡‡]Radiation requires no medium to transmit energy.

where, for brevity, we denote $\boldsymbol{r}_i^{L+1} \stackrel{\text{def}}{=} \boldsymbol{r}_i(t+\Delta t)$, $\boldsymbol{r}_i^{L} \stackrel{\text{def}}{=} \boldsymbol{r}_i(t)$ etc., one can arrive at the following abstract form, for the entire system, $\mathscr{A}(\boldsymbol{r}^{L+1}) = \mathscr{F}$. It is convenient to write

$$\mathscr{A}(\boldsymbol{r}^{L+1}) - \mathscr{F} = \mathscr{G}(\boldsymbol{r}^{L+1}) - \boldsymbol{r}^{L+1} + \mathscr{E} = \boldsymbol{0} \tag{46}$$

where $\mathscr{E}$ is a remainder term which does not depend on the solution, i.e. $\mathscr{E} \neq \mathscr{E}(\boldsymbol{r}^{L+1})$. A straightforward iterative scheme can be written as

$$\boldsymbol{r}^{L+1,K} = \mathscr{G}(\boldsymbol{r}^{L+1,K-1}) + \mathscr{E} \tag{47}$$

where $K = 1, 2, 3, \ldots$ is the index of iteration within time-step $L+1$. The convergence of such a scheme is dependent on the behaviour of $\mathscr{G}$. Namely, a sufficient condition for convergence is that $\mathscr{G}$ is a contraction mapping for all $\boldsymbol{r}^{L+1,K}$, $K = 1, 2, 3 \ldots$. In order to investigate this further, we define the error as $\varepsilon^{L+1,K} = \boldsymbol{r}^{L+1,K} - \boldsymbol{r}^{L+1}$. A necessary restriction for convergence is iterative self consistency, i.e. the exact solution must be represented by the scheme $\mathscr{G}(\boldsymbol{r}^{L+1}) + \mathscr{E} = \boldsymbol{r}^{L+1}$. Enforcing this restriction, a sufficient condition for convergence is the existence of a contraction mapping of the form

$$\|\varepsilon^{L+1,K}\| = \|\boldsymbol{r}^{L+1,K} - \boldsymbol{r}^{L+1}\| = \|\mathscr{G}(\boldsymbol{r}^{L+1,K-1}) - \mathscr{G}(\boldsymbol{r}^{L+1})\| \leqslant \eta^{L+1,K}\|\boldsymbol{r}^{L+1,K-1} - \boldsymbol{r}^{L+1}\| \tag{48}$$

where, if $\eta^{L+1,K} < 1$ for each iteration K, then $\varepsilon^{L+1,K} \to \boldsymbol{0}$ for any arbitrary starting value $\boldsymbol{r}^{L+1,K=0}$ as $K \to \infty$. The type of contraction condition discussed is sufficient, but not necessary, for convergence. In order to control convergence, we modify the discretization of the acceleration term:

$$\ddot{\boldsymbol{r}}^{L+1} \approx \frac{\dot{\boldsymbol{r}}^{L+1} - \dot{\boldsymbol{r}}^{L}}{\Delta t} \approx \frac{\frac{\boldsymbol{r}^{L+1} - \boldsymbol{r}^{L}}{\Delta t} - \dot{\boldsymbol{r}}^{L}}{\Delta t} \approx \frac{\boldsymbol{r}^{L+1} - \boldsymbol{r}^{L}}{\Delta t^2} - \frac{\dot{\boldsymbol{r}}^{L}}{\Delta t} \tag{49}$$

which collapses to the familiar difference stencil of $\ddot{\boldsymbol{r}}^{L+1} = (\boldsymbol{r}^{L+1} - 2\boldsymbol{r}^{L} + \boldsymbol{r}^{L-1})/(\Delta t)^2$, when the time-step size is uniform. Inserting this into $m\ddot{\boldsymbol{r}} = \boldsymbol{\Psi}^{\text{tot}}(\boldsymbol{r})$ leads to

$$\boldsymbol{r}^{L+1,K} \approx \underbrace{\frac{\Delta t^2}{m}(\boldsymbol{\Psi}^{\text{tot}}(\boldsymbol{r}^{L+1,K-1}))}_{\mathscr{G}(\boldsymbol{r}^{L+1,K-1})} + \underbrace{(\boldsymbol{r}^{L} + \Delta t\dot{\boldsymbol{r}}^{L})}_{\mathscr{E}} \tag{50}$$

whose convergence is restricted by $\eta \propto \text{EIG}(\mathscr{G}) \propto \Delta t^2/m$. Thus, decreasing the time-step size improves the convergence, however, we want to simultaneously maximize the time-step sizes to decrease overall computing time, while still meeting an error tolerance. In order to achieve this goal, we follow an approach in References [75, 76] initially developed for continuum thermo-chemical multifield problems in which (1) one approximates $\eta^{L+1,K} \approx S(\Delta t)^p$ (S is a constant) and (2) one approximates the error within an iteration to behave according to $(S(\Delta t)^p)^K\|\varepsilon^{L+1,0}\| = \|\varepsilon^{L+1,K}\|$, $K = 1, 2, \ldots$, where $\|\varepsilon^{L+1,0}\|$ is the initial norm of

the iterative error and S is a function intrinsic to the system.[§§§] Our goal is to meet an error tolerance in exactly a preset number of iterations. To this end, one writes this in the following approximate form, $(S(\Delta t_{\text{tol}})^p)^{K_{\text{d}}}\|\varepsilon^{L+1,0}\| = \text{TOL}$, where TOL is a tolerance and where K_{d} is the number of desired iterations.[¶¶¶] If the error tolerance is not met in the desired number of iterations, the contraction constant $\eta^{L+1,K}$ is too large. Accordingly, one can solve for a new smaller step size, under the assumption that S is constant,

$$\Delta t_{\text{tot}} = \Delta t \left(\frac{\left(\dfrac{\text{TOL}}{\|\varepsilon^{L+1,0}\|} \right)^{1/pK_{\text{d}}}}{\left(\dfrac{\|\varepsilon^{L+1,K}\|}{\|\varepsilon^{L+1,0}\|} \right)^{1/pK}} \right) \tag{51}$$

The assumption that S is constant is not critical, since the time-steps are to be recursively refined and unrefined repeatedly. Clearly, the previous expression can also be used for time-step enlargement, if convergence is met in less than K_{d} iterations. Time-step size adaptivity is paramount, since the flow's dynamics can dramatically change over the course of time, requiring radically different time-step sizes for a preset level of accuracy. However, one must respect an upper bound dictated by the discretization error, i.e. $\Delta t \leqslant \Delta t^{\text{lim}}$. In order to couple this to the thermo-chemical computations, we define the normalized errors within each time-step, for the two fields,

$$\varepsilon_{rK} \stackrel{\text{def}}{=} \frac{\|\boldsymbol{r}^{L+1,K} - \boldsymbol{r}^{L+1,K-1}\|}{\|\boldsymbol{r}^{L+1,K}\|} \quad \text{and} \quad \varepsilon_{\theta K} \stackrel{\text{def}}{=} \frac{\|\theta^{L+1,K} - \theta^{L+1,K-1}\|}{\|\theta^{L+1,K}\|} \tag{52}$$

We define 'violation ratios', i.e. measure of which field is relatively more in error, compared to its corresponding tolerance, i.e. $Z_K \stackrel{\text{def}}{=} \max(z_{rK}, z_{\theta K})$ where

$$z_{rK} \stackrel{\text{def}}{=} \frac{\varepsilon_{rK}}{\text{TOL}_r} \quad \text{and} \quad z_{\theta K} \stackrel{\text{def}}{=} \frac{\varepsilon_{\theta K}}{\text{TOL}_\theta} \tag{53}$$

and a minimum scaling factor $\Phi_K \stackrel{\text{def}}{=} \min(\phi_{rK}, \phi_{\theta K})$ from

$$\phi_{rK} \stackrel{\text{def}}{=} \left(\frac{\left(\dfrac{\text{TOL}_r}{\varepsilon_{r0}} \right)^{1/pK_{\text{d}}}}{\left(\dfrac{\varepsilon_{rK}}{\varepsilon_{r0}} \right)^{1/pK}} \right), \quad \phi_{\theta K} \stackrel{\text{def}}{=} \left(\frac{\left(\dfrac{\text{TOL}_\theta}{\varepsilon_{\theta 0}} \right)^{1/pK_{\text{d}}}}{\left(\dfrac{\varepsilon_{\theta K}}{\varepsilon_{\theta 0}} \right)^{1/pK}} \right) \tag{54}$$

[§§§] For the class of problems under consideration, due to the quadratic dependency on Δt, $p \approx 2$.
[¶¶¶] Typically, K_{d} is chosen to be between five and ten iterations.

The algorithm is as follows:

(1) GLOBAL FIXED – POINT ITERATION: (SET $i = 1$ AND $K = 0$):
(2) IF $i > n$ THEN GO TO (4)
(3) IF $i \leqslant n$ THEN:

(a) COMPUTE POSITION: $\boldsymbol{r}_i^{L+1,K} = \dfrac{\Delta t^2}{m_i}\,(\boldsymbol{\Psi}_i^{\mathrm{tot}}(\boldsymbol{r}^{L+1,K-1})) + \boldsymbol{r}_i^{L} + \Delta t \dot{\boldsymbol{r}}_i^{L}$

(b) COMPUTE TEMPERATURE:

$$\theta_i^{L+1,K} = \theta_i^{L} + \frac{\delta \mathscr{H}_i^{L+1,K}}{m_i C}.$$

$$\theta_i^{L+1,K} = \frac{mC}{mC + h_{\mathrm{c}} a_{\mathrm{s}} \Delta t}\,\theta_i^{L+1,K} - \frac{\Delta t \mathscr{B} a_{\mathrm{s}} \varepsilon}{mC + h_{\mathrm{c}} a_{\mathrm{s}} \Delta t}\,((\theta_i^{L+1,K})^4 - \theta_{\mathrm{s}}^4) + \frac{h_{\mathrm{c}} a_{\mathrm{s}} \Delta t\, \theta_0}{mC + h_{\mathrm{c}} a_{\mathrm{s}} \Delta t}$$

(c) GO TO (2) AND NEXT FLOW PARTICLE ($i = i + 1$)

(4) ERROR MEASURES:

(a) $\varepsilon_{rK} \overset{\mathrm{def}}{=} \dfrac{\sum_{i=1}^{n} \|\boldsymbol{r}_i^{L+1,K} - \boldsymbol{r}_i^{L+1,K-1}\|}{\sum_{i=1}^{n} \|\boldsymbol{r}_{iL+1,K}\|}$ $\qquad \varepsilon_{\theta K} \overset{\mathrm{def}}{=} \dfrac{\sum_{i=1}^{n} \|\theta_i^{L+1,K} - \theta_i^{L+1,K-1}\|}{\sum_{i=1}^{n} \|\theta_i^{L+1,K}\|}.$

(b) $Z_K \overset{\mathrm{def}}{=} max(z_{rK}, z_{\theta K})$ *where* $z_{rK} \overset{\mathrm{def}}{=} \dfrac{\varepsilon_{rK}}{\mathrm{TOL}_r}$, $z_{\theta K} \overset{\mathrm{def}}{=} \dfrac{\varepsilon_{\theta K}}{\mathrm{TOL}_\theta}$

(c) $\Phi_K \overset{\mathrm{def}}{=} min(\phi_{rK}, \phi_{\theta K})$ *where* $\phi_{rK} \overset{\mathrm{def}}{=} \left(\dfrac{\left(\dfrac{\mathrm{TOL}_r}{\varepsilon_{r0}}\right)^{\frac{1}{pK_{\mathrm{d}}}}}{\left(\dfrac{\varepsilon_{rK}}{\varepsilon_{r0}}\right)^{\frac{1}{pK}}} \right)$, $\phi_{\theta K} \overset{\mathrm{def}}{=} \left(\dfrac{\left(\dfrac{\mathrm{TOL}_\theta}{\varepsilon_{\theta 0}}\right)^{\frac{1}{K_{pd}}}}{\left(\dfrac{\varepsilon_{\theta K}}{\varepsilon_{\theta 0}}\right)^{\frac{1}{pK}}} \right)$

(5) IF TOLERANCE MET ($Z_K \leqslant 1$) AND $K < K_{\mathrm{d}}$ THEN:

(a) CONSTRUCT NEW TIME STEP: $\Delta t = \Phi_K \Delta t$,
(b) SELECT MINIMUM: $\Delta t = \mathrm{MIN}(\Delta t^{\mathrm{lim}}, \Delta t)$
(c) INCREMENT TIME: $t = t + \Delta t$ AND GO TO (1)

(6) IF TOLERANCE NOT MET ($Z_K > 1$) AND $K = K_{\mathrm{d}}$ THEN:

(a) CONSTRUCT NEW TIME STEP: $\Delta t = \Phi_K \Delta t$
(b) RESTART AT TIME = t AND GO TO (1)

(55)

Remark 1

We remark that the forces needed to compute terms in coefficient of restitution e, for example E_{in}, E_{jn} and D_{ij} are computed via by using the most currently known values of the $\boldsymbol{\Psi}_i$'s during the iterative solution process. In other words, the interaction forces are updated during the iterations, within a time-step, based on the most currently known positions of the particles. This process includes testing whether $\|\boldsymbol{r}_i - \boldsymbol{r}_j\| \leqslant b_i + b_j$, which is a check for contact between particles. The purpose of the algorithm is to deliver solutions where the coupling is resolved in an iterative manner, by the recursive sequential solution of the various field equations,

constraints, etc. The incomplete coupling error is controlled by adaptively controlling the time-step sizes, while the temporal discretization accuracy dictates the upper limit on the time-step size ($\Delta t^{\lim}$).

Remark 2
We note that Equation (42) is of the form

$$\theta(t+\Delta t) = \mathscr{G}(\theta(t+\Delta t)) + \mathscr{E} \tag{56}$$

where $\mathscr{E} \neq \mathscr{E}(\theta(t+\Delta t))$, and where $\mathscr{G}$'s behaviour is controlled by $\frac{\Delta t \mathscr{B} a_s \varepsilon}{mC + h_c a_s \Delta t}$, which is quite small. Thus, a fixed-point iterative scheme such as $\theta^K(t+\Delta t) = \mathscr{G}(\theta^{K-1}(t+\Delta t)) + \mathscr{E}$, converges rapidly.

Remark 3
One could attempt to solve the entire system simultaneously (monolithically). This would likely involve the use of a gradient-based scheme, which can also be considered as a type of fixed-point iteration. For example, Newton's method is covered as a special case of this general analysis. To see this, let $\boldsymbol{w} = (\boldsymbol{r}, \theta)$, and consider the residual defined by $\boldsymbol{\Pi} \stackrel{\text{def}}{=} \mathscr{A}(\boldsymbol{w}) - \mathscr{F}$, which upon linearization yields

$$\boldsymbol{\Pi}(\boldsymbol{w}^K) = \boldsymbol{\Pi}(\boldsymbol{w}^{K-1}) + \nabla_{\boldsymbol{w}} \boldsymbol{\Pi}_{\boldsymbol{w}^{K-1}} (\boldsymbol{w}^K - \boldsymbol{w}^{K-1}) + \mathscr{O}(\|\Delta \boldsymbol{w}\|^2) \tag{57}$$

An updating (Newton) scheme can be developed by setting $\boldsymbol{\Pi}(\boldsymbol{w}^K) \approx 0$, leading to

$$\boldsymbol{w}^K = \boldsymbol{w}^{K-1} - (\mathscr{A}^{\text{TAN},K-1})^{-1} \boldsymbol{\Pi}(\boldsymbol{w}^{K-1}) \tag{58}$$

where the tangent is

$$\mathscr{A}^{\text{TAN},K} = (\nabla_{\boldsymbol{w}} \mathscr{A}(\boldsymbol{w}))|_{\boldsymbol{w}^K} = (\nabla_{\boldsymbol{w}} \boldsymbol{\Pi}(\boldsymbol{w}))|_{\boldsymbol{w}^K} \tag{59}$$

Therefore, in a fixed-point form one has the operator $\mathscr{G}(\boldsymbol{w}) = \boldsymbol{w} - (\mathscr{A}^{\text{TAN}})^{-1} \boldsymbol{\Pi}(\boldsymbol{w})$. The gradient is

$$\nabla_{\boldsymbol{w}} \mathscr{G}(\boldsymbol{w}) = (\mathscr{A}^{\text{TAN}})^{-2} (\mathscr{A}^{\text{TAN}})^{\text{TAN}} \boldsymbol{\Pi}(\boldsymbol{w}) \tag{60}$$

where $(\mathscr{A}^{\text{TAN}})^{\text{TAN}} \stackrel{\text{def}}{=} \nabla_{\boldsymbol{w}} (\nabla_{\boldsymbol{w}} \mathscr{A}(\boldsymbol{w}))$. The convergence criteria is, $\forall K = 1, 2, \ldots$, following the approach for the first fixed-point scheme:

$$\|\mathscr{G}(\boldsymbol{w}^{K-1}) - \mathscr{G}(\boldsymbol{w})\| \leqslant \underbrace{\|(\mathscr{A}^{\text{TAN},K-1})^{-2} (\mathscr{A}^{\text{TAN},K-1})^{\text{TAN},K-1} \boldsymbol{\Pi}(\boldsymbol{w}^{K-1})\|}_{\eta} \|\boldsymbol{w}^{K-1} - \boldsymbol{w}\| \tag{61}$$

Equivalently, one can write $\|((\nabla_{\boldsymbol{w}} \boldsymbol{\Pi})^{-2} \nabla_{\boldsymbol{w}} (\nabla_{\boldsymbol{w}} \boldsymbol{\Pi}(\boldsymbol{\Pi}(\boldsymbol{w}))))|_{\boldsymbol{w}^{K-1}}\| < 1$. A serious difficulty is likely, due to the possibility of a zero, or near zero, tangent when employing a Newton's method to a non-convex system, which can lose positive definiteness. This will, in turn, lead to an indefinite-type system of algebraic equations. Therefore, while Newton's method usually converges at a faster rate than a direct fixed point iteration, quadratic as opposed to superlinear, its convergence criteria is less robust than the presented fixed-point algorithm, due to its dependence on the gradients of the solution. Furthermore, for the problems considered, it is unlikely that the gradients of $\mathscr{G}$ remain positive definite, or even that $\mathscr{G}$ is continuously differentiable, due to the impact events, and thus we employed a staggering scheme which

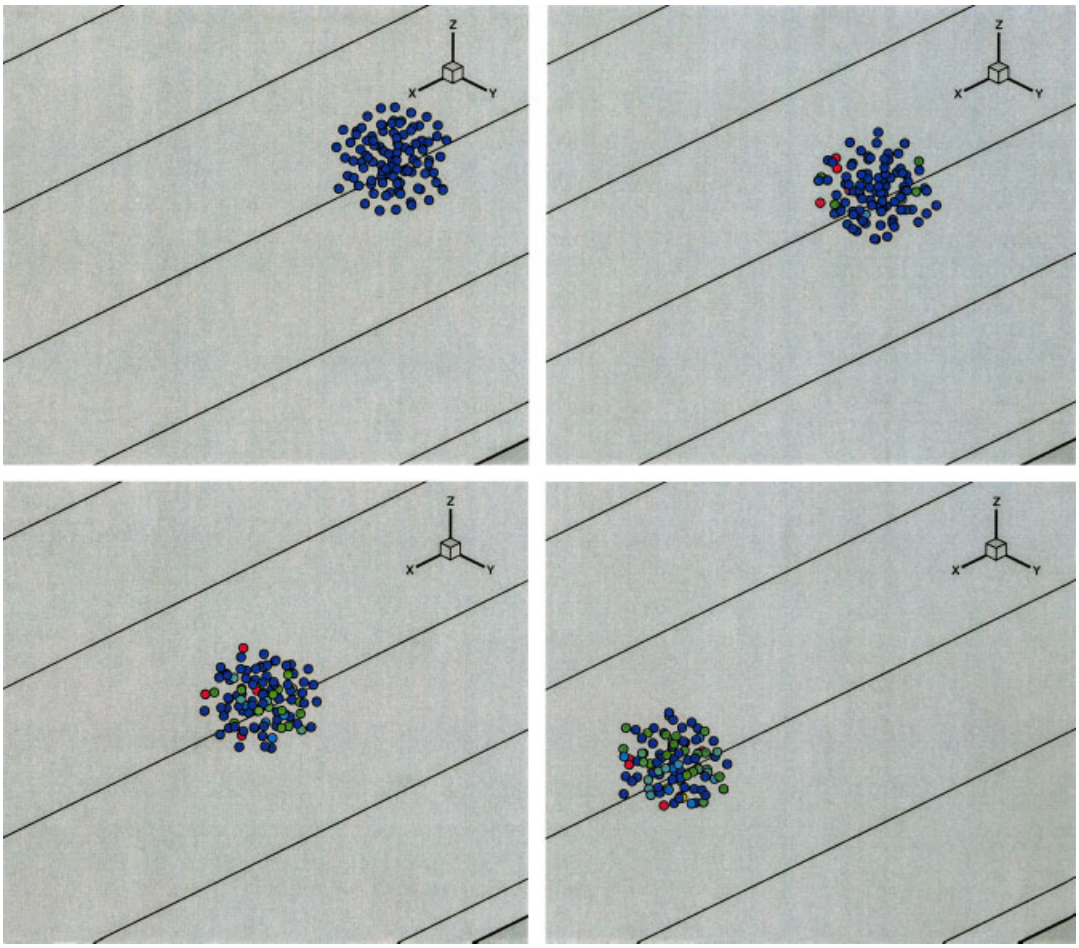

Figure 4. Starting from left to right and top to bottom, the dynamics of the particulate flow *without clustering forces*. Blue (lowest) indicates a temperature of approximately 300 K, while red (highest) indicated a temperature of approximately 400 K.

avoided the use of gradients. Thus, in summary, there are a variety of difficulties with such a gradient-based approach: (1) The computations are not easily parallelizable, (2) Classical gradient-based algorithms are likely to converge only if an accurate initial guess is provided and, usually, it is extremely difficult to construct an initial guess that lies within a convergence radius of a gradient-based method and (3) The system behaviour is non-convex and non-differentiable with respect to the positions and temperatures of the particles.

6. NUMERICAL SIMULATION

In order to simulate a particulate flow, we considered a group of n randomly positioned particles, of equal size, in a (starting) cube of normalized dimensions, $D \times D \times D$, with D normalized to

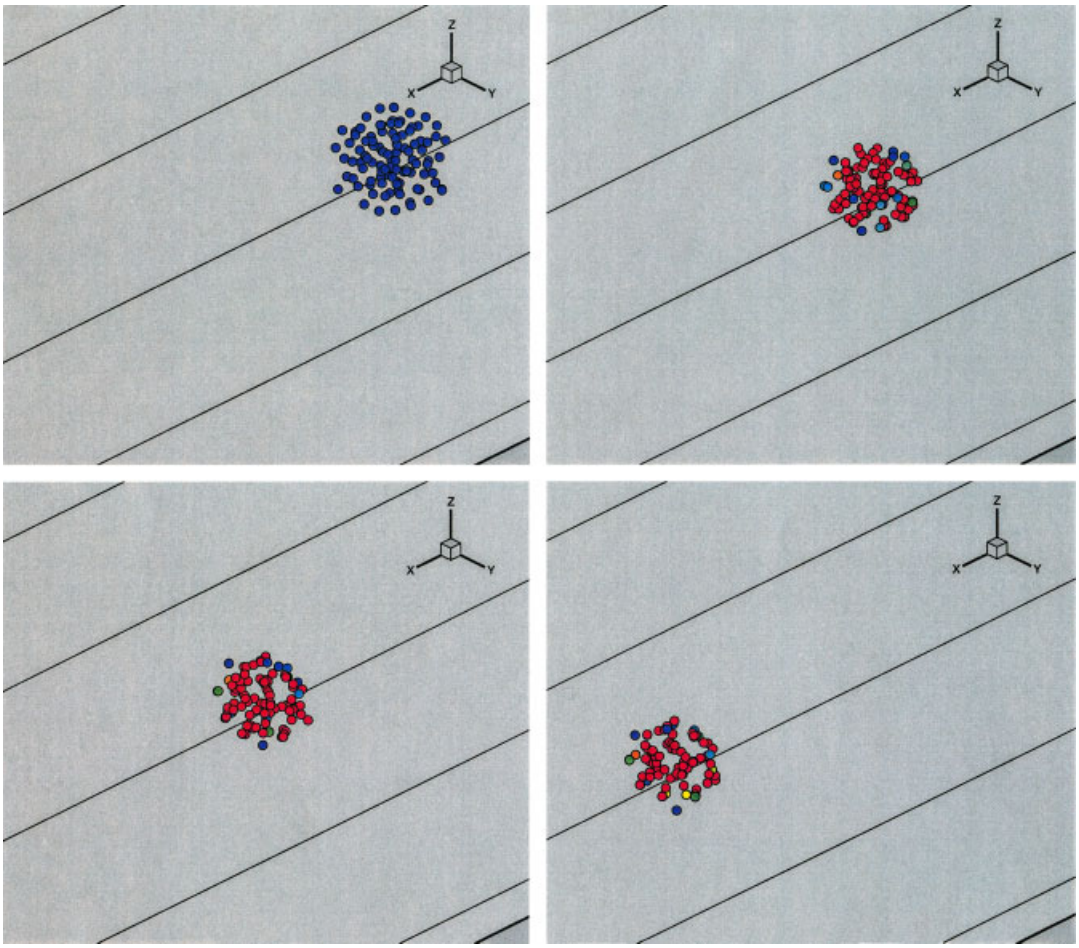

Figure 5. Starting from left to right and top to bottom, the dynamics of the particulate flow *with clustering forces*: An initially fine cloud of particles which clusters to form structures within the flow. Blue (lowest) indicates a temperature of approximately 300 K, while red (highest) indicates a temperature of approximately 400 K.

unity. The particle size and volume fraction were determined by a particle/sample size ratio, which was defined via a subvolume size $V \stackrel{\text{def}}{=} D \times D \times D/n$, where n was the number of particles in the entire cube. The ratio between the radius (b) and the subvolume was denoted by $\mathscr{L} \stackrel{\text{def}}{=} \frac{b}{V^{1/3}}$. The volume fraction occupied by the particles was $v_f \stackrel{\text{def}}{=} 4\pi\mathscr{L}^3/3$. Thus, the total volume occupied by the particles, denoted ζ, could be written as $\zeta = v_f nV$, and the total mass written as $M = \sum_{i=1}^{n} m_i = \rho\zeta$, while that of an individual particle, assuming that all are the same size, was $m_i = \frac{\rho\zeta}{n} = \rho\,\frac{4}{3}\pi b_i^3$. In order to visualize the flow clearly, we used $n = 100$ particles. The length scale of the particles was $\mathscr{L} = 0.25$, which resulted in a corresponding volume fraction of $v_f = 4\pi\mathscr{L}^3/3 = 0.0655$ and particulate radii of $b = 0.0539$. A mass

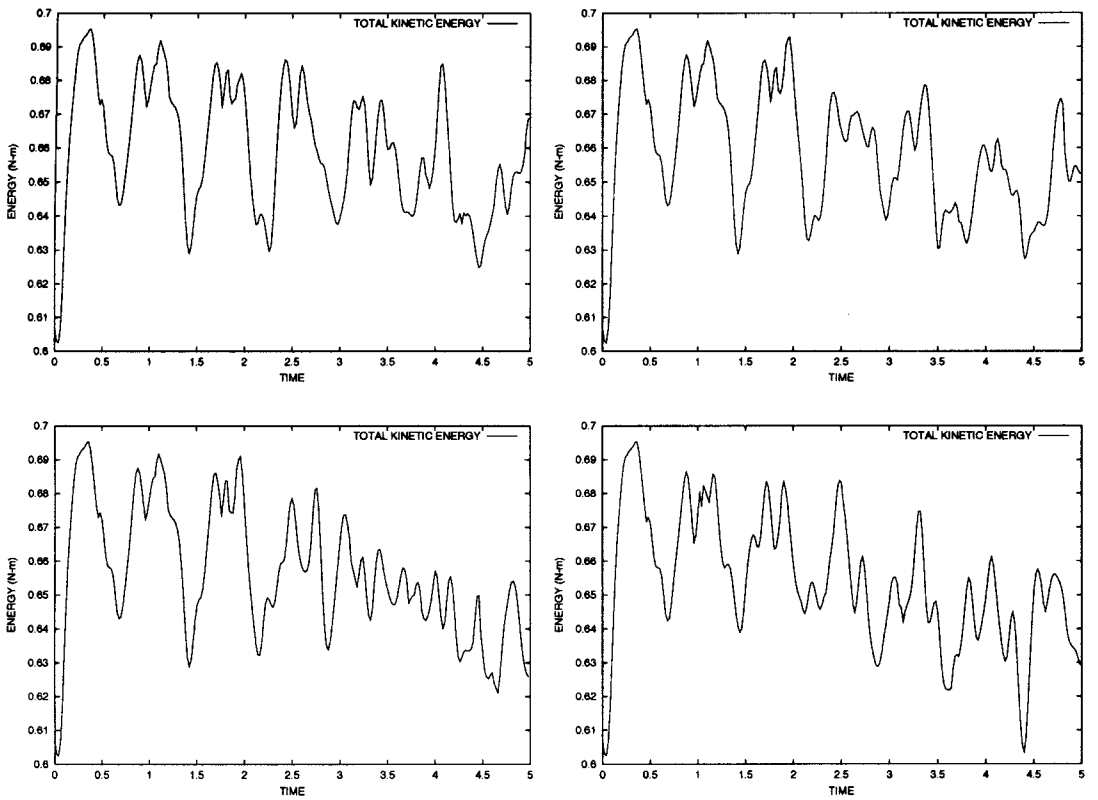

Figure 6. Starting from left to right and top to bottom, *without clustering forces*: the total kinetic energy in the system per unit mass with $e_0 = 0.5$, $\mu_s = 0.2$, $\mu_d = 0.1$, $\bar{\alpha}_1 = 0.5$ and $\bar{\alpha}_2 = 0.25$: (1) $\kappa = 10^6\,\mathrm{J/m^2}$, (2) $\kappa = 2 \times 10^6\,\mathrm{J/m^2}$, (3) $\kappa = 4 \times 10^6\,\mathrm{J/m^2}$, and (4) $\kappa = 8 \times 10^6\,\mathrm{J/m^2}$.

density of the particles $= 2000\,\mathrm{kg/m^3}$ was used. The ambient temperature was selected to be $\theta_0 = \theta_s = 300\,\mathrm{K}$. The heat capacity of the particles was $\mathscr{C} = 10^3\,\mathrm{J/kg\,K}$, with emissivity of $\varepsilon = 10^{-2}$. The critical temperature parameter in the coefficient of restitution relation was $\theta^* = 3000\,\mathrm{K}$. The reaction constant was varied between $10^6\,\mathrm{J/m^2} \leqslant \kappa \leqslant 10^7\,\mathrm{J/m^2}$, with $I^* = 10^3\,\mathrm{N}$. The coefficient of convective heat transfer (h_c) was set to zero. We introduced the following near-field parameter per unit $mass^2$ $\alpha_{1ij} = \bar{\alpha}_1 m_i m_j$, $\alpha_{2ij} = \bar{\alpha}_2 m_i m_j$ and $\alpha_{aij} = \bar{\alpha}_a m_i m_j$. This allowed one to scale the strength of the interaction forces according to the mass of the particles.[‖‖‖‖] The initial mean velocity field, componentwise, was $(1.0, 0.1, 0.1)\,\mathrm{m/s}$ with initial random perturbations around mean velocity of $(\pm 1.0, \pm 0.1, \pm 0.1)\,\mathrm{m/s}$, and a critical threshold velocity of $10\,\mathrm{m/s}$ in Equation (35). The simulation duration was set to five seconds, with an upper bound on the time-step size of $\Delta t^{\lim} = 10^{-2}\,\mathrm{s}$ and a starting time-step size of $10^{-3}\,\mathrm{s}$.

[‖‖‖‖]Although, we did not consider particles of different sizes in the present work, this decomposition allows one to easily take this into account. Also, we enforced the near-field stability condition by setting $(\beta_1, \beta_2) = (1, 2)$.

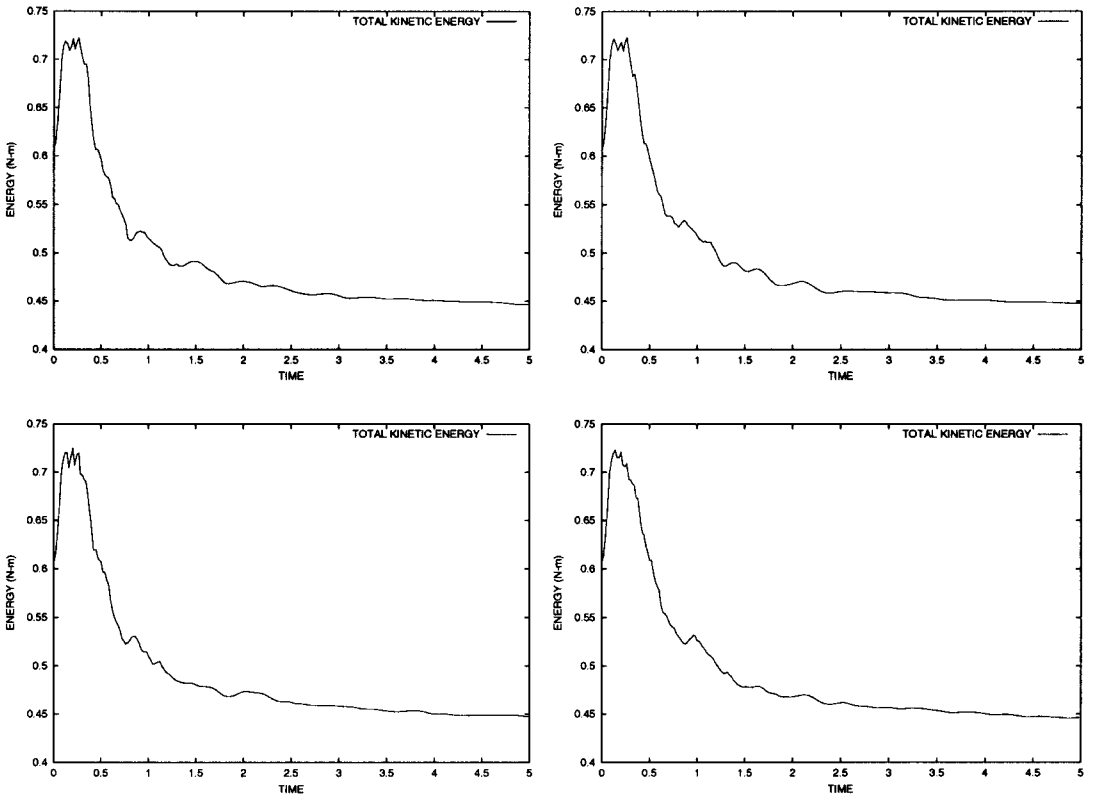

Figure 7. Starting from left to right and top to bottom, *with clustering forces*: the total kinetic energy in the system per unit mass with $e_0 = 0.5$, $\mu_s = 0.2$, $\mu_d = 0.1$, $\bar{\alpha}_1 = 0.5$ and $\bar{\alpha}_2 = 0.25$: (1) $\kappa = 10^6 \mathrm{J/m^2}$, (2) $\kappa = 2 \times 10^6 \mathrm{J/m^2}$, (3) $\kappa = 4 \times 10^6 \mathrm{J/m^2}$, and (4) $\kappa = 8 \times 10^6 \mathrm{J/m^2}$.

The tolerances of both fields (TOL_r and TOL_θ) for the fixed-point iterations were set to 10^{-6} and the upper limit on the number of fixed-point iterations was set to $k^{\mathrm{d}} = 10^2$.

Two main types of computational tests were conducted:

1. Varying κ, for a given field strength, $\bar{\alpha}_1 = 0.5$ and $\bar{\alpha}_2 = 0.25$, with a clustering augmentation of $\bar{\alpha}_a = 1.75$ (forcing a small gap characterized by $d_a = 1.03(2b)$), $\beta_a = 1$, $\delta_a = 1.65(2b)$.
2. Varying κ, for a given field strength, $\bar{\alpha}_1 = 0.5$ and $\bar{\alpha}_2 = 0.25$, without a clustering augmentation.

For each different parameter selection, the initial conditions, i.e. random positions, velocities, temperatures, etc., were the same. We remark that parameter studies on the near-field strength, in isolation (without thermo-chemical coupling), have been conducted in Reference [54]. The field strength chosen was strong enough to induce vibratory motion, and hence, non-monotone kinetic energy. Frames of the flows for cases (1) and (2), for typical values of $\kappa = 2 \times 10^6 \mathrm{J/m^2}$, are shown in Figures 4 and 5. The plots in Figures 6–9 indicate the overall energetic and thermal

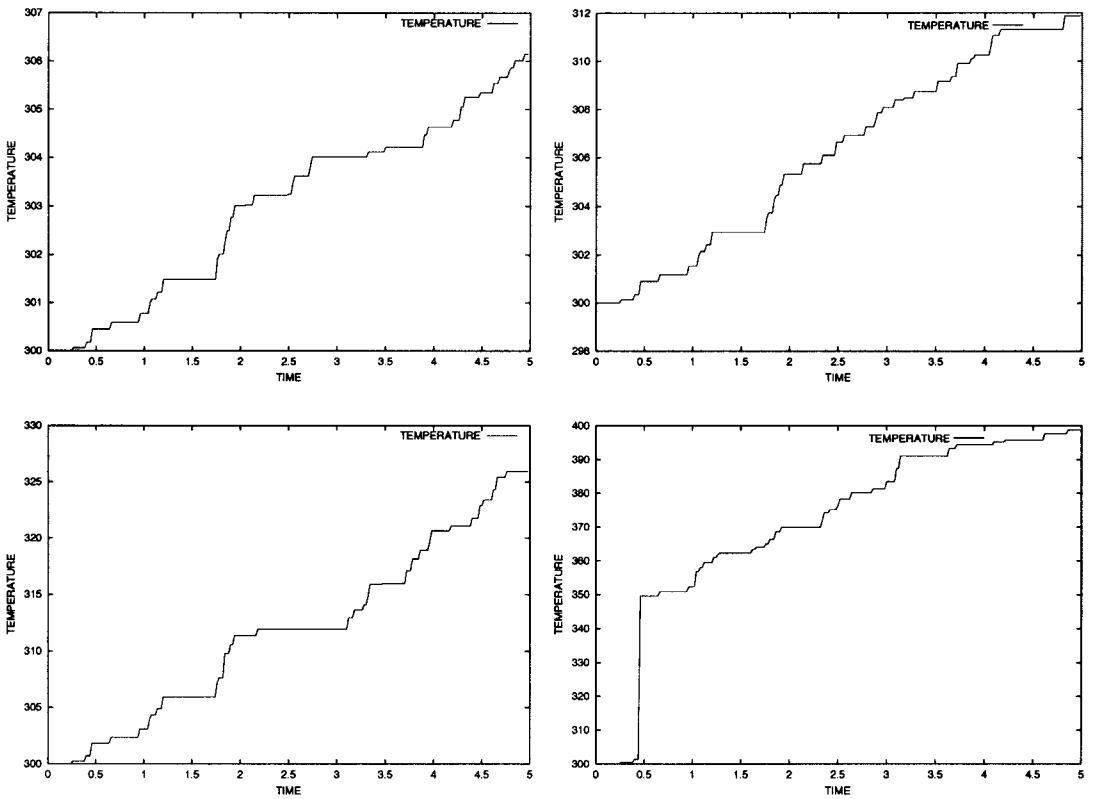

Figure 8. Starting from left to right and top to bottom, *without clustering forces*: the average particle temperature with $e_0 = 0.5$, $\mu_s = 0.2$, $\mu_d = 0.1$, $\bar{\alpha}_1 = 0.5$ and $\bar{\alpha}_2 = 0.25$: (1) $\kappa = 10^6\,\mathrm{J/m^2}$, (2) $\kappa = 2 \times 10^6\,\mathrm{J/m^2}$, (3) $\kappa = 4 \times 10^6\,\mathrm{J/m^2}$, and (4) $\kappa = 8 \times 10^6\,\mathrm{J/m^2}$.

behaviour. Typically, the simulations took approximately between 1 and 2 min on a standard (Dell, 2.33 GHz) laptop.**** For the parameter ranges used in the presented simulations, the degree of adaptivity needed strongly depended on the presence of the clustering forces, and to a somewhat lesser degree on the thermo-chemical parameters. For example, for the 5 s simulation, if the time-steps stayed at the starting value ($\Delta t = 10^{-3}$ s), then 5000 time-steps would be needed, if there had been no time-step adaptivity (time-step enlargement). Conversely, if the time-steps were found to be unnecessarily too small (an overkill) at the starting value ($\Delta t = 10^{-3}$ s), and, consequently, unrefined to the upper bound ($\Delta t^{\lim} = 10^{-2}$ s), then approximately 500 time-steps would be needed. Tables I and II indicate that, for the parameter ranges tested, when clustering forces were not present, the time-steps did not need to be refined, nor unrefined. However, when clustering forces were present, the time-steps could be unrefined for the given

****The computation time scales, approximately, no worse than the number of particles squared. For example, a thousand particles took approximately 15 min.

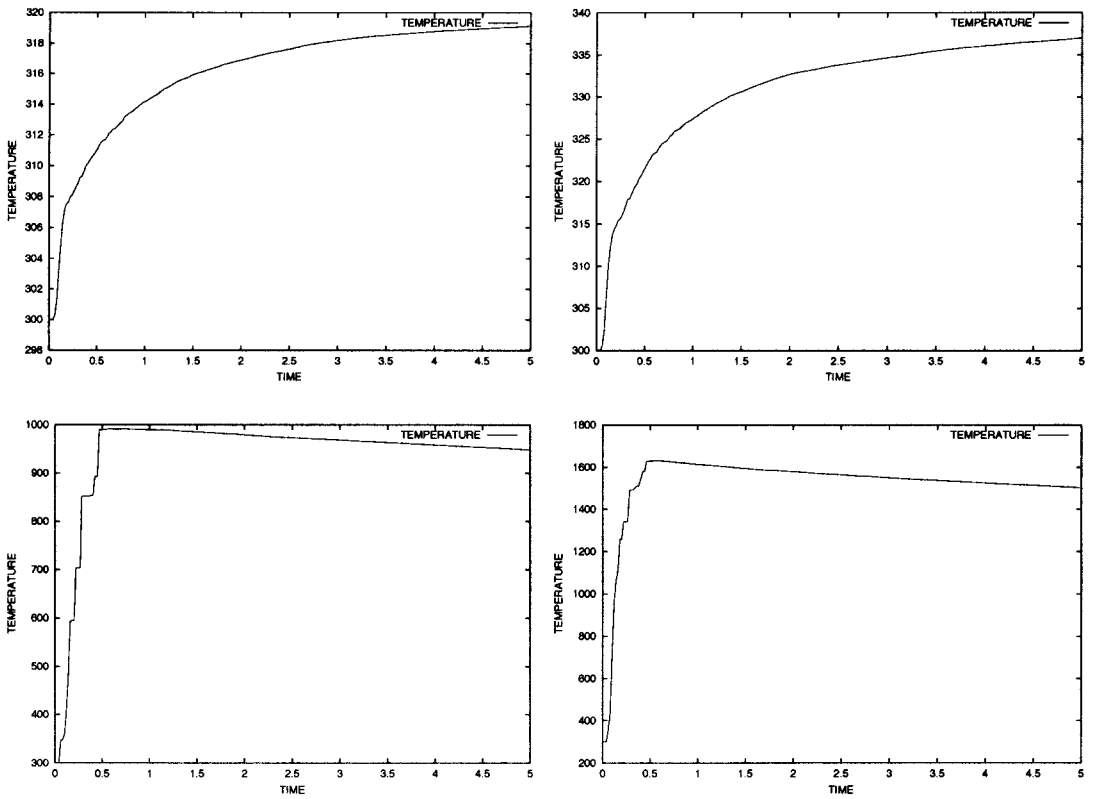

Figure 9. Starting from left to right and top to bottom, *with clustering forces*: the average particle temperature with $e_0 = 0.5$, $\mu_s = 0.2$, $\mu_d = 0.1$, $\bar{\alpha}_1 = 0.5$ and $\bar{\alpha}_2 = 0.25$: (1) $\kappa = 10^6\ \mathrm{J/m^2}$, (2) $\kappa = 2 \times 10^6\ \mathrm{J/m^2}$, (3) $\kappa = 4 \times 10^6\ \mathrm{J/m^2}$, and (4) $\kappa = 8 \times 10^6\ \mathrm{J/m^2}$.

Table I. The number of time-steps and fixed-point iterations, without clustering forces: the average particle temperature with $e_0 = 0.5$, $\mu_s = 0.2$, $\mu_d = 0.1$, $\bar{\alpha}_1 = 0.5$ and $\bar{\alpha}_2 = 0.25$.

κ $(J \times 10^6/\mathrm{m}^2)$	Time-steps	Fixed-point iterations
1	5000	5037
2	5000	5038
4	5000	5037
8	5000	5032

tolerances, however, requiring more internal fixed-point iterations. This was primarily because cluster-structures formed, leading to less collisions between the larger objects, which did not require such small time-steps (Figure 10). For the simulations with clustering forces, there was an expected thermal sensitivity. As the reaction term κ became stronger, the number

Table II. The number of time-steps and fixed-point iterations, with clustering forces: the average particle temperature with $e_0 = 0.5$, $\mu_s = 0.2$, $\mu_d = 0.1$, $\bar{\alpha}_1 = 0.5$ and $\bar{\alpha}_2 = 0.25$.

κ $(J \times 10^6/\mathrm{m}^2)$	Time-steps	Fixed-point iterations
1	586	1735
2	585	1798
4	548	5147
8	601	5565

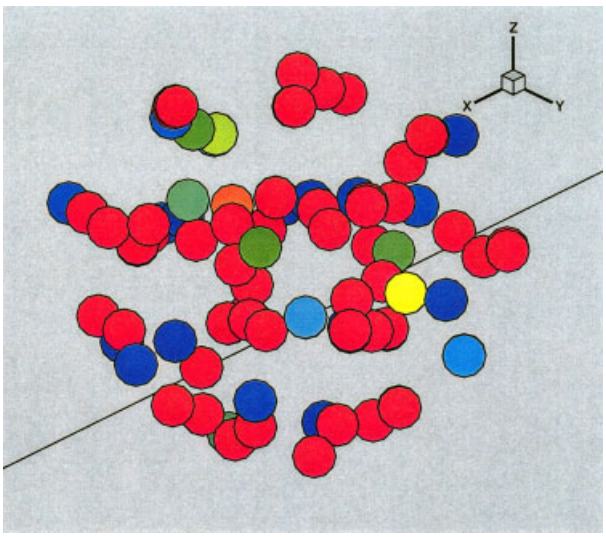

Figure 10. A zoom on the structures that form *with clustering*. Blue (lowest) indicates a temperature of approximately 300 K, while red (highest) indicates a temperature of approximately 400 K.

of fixed-point iterations required to achieve convergence increased. These results highlight an essential point of the adaptive process, which is to allow the system to adjust to the physics of the problem. Some further remarks elaborating on this issue can be found in References [54, 75, 76].

Qualitatively speaking, one should expect that when a clustering field becomes active between two approaching particles, then kinetic energy is lost because of the disappearance of normal relative velocities between them. Conversely, kinetic energy is gained if the particles become dislodged, because the clustering field becomes inactive and the repulsive field suddenly dominates the remaining attractive forces, thus pushing the previously clustered particles away from one another. When the clustering binding field becomes active, the coefficient of restitution will play virtually no role, because the strength of the attractive this force dominates everything. Thus, because the thermal field affects the particle dynamics through the coefficient of restitution, when clustering dominates, the particle dynamics will be only marginally affected by varying κ (Figure 7). However, the temperature of the particles, in the presence

of clustering will rise substantially, due to the large compressive forces between the contacting particles, which activates the chemical reactions. Also, we remark that the group dynamics, for different κ without clustering forces, deviate much more from one another than the cases when clustering is present (Figure 6). Typically, when two particles have clustered, since the binding field was strong, the particles rarely become dislodged.

7. CONCLUDING REMARKS

Experimentally speaking, thermal behaviour can be a key indicator of the dynamical character of the flow. For example, in References [86, 87], techniques for measuring flow characteristics based upon Infrared Thermal Velocimetry (ITV) in fluidic microelectromechanical systems (MEMS) have been developed. In such approaches infrared lasers are used to generate a short heating pulse in a flowing liquid, and an infrared camera records the radiative images from the heated flowing liquid. The flow properties are obtained from consecutive radiative images. This approach is robust enough to measure particulate flows as well. We remark that thermal flow sensors, based on a 'time of flight' principle, are also possible [88]. In such approaches, a heater generates a short thermal pulse, and a thermal sensor detects the arrival downstream. The author is currently engaged in collaboration with experimentalists in order to test and fine-tune the presented model. Accordingly, an important aspect of the model, or any particulate flow model, is parameter identification. For example, consider a cost function of the form $\Pi = \int_0^{\mathscr{T}} |A - A^*| \, \mathrm{d}t$, where total simulation or experimental time is $\mathscr{T}$, where A is a computationally or experimentally generated quantity of interest and where A^* is the target or observed response. The objective is to minimize Π by determining feasible system parameters such as near-field coefficients, $\bar{\alpha}_1$, β_1, $\bar{\alpha}_2$ and β_2, reaction constants such as κ, friction parameters such as μ_s and μ_d, etc. Typically, Π depends in a non-convex and non-differentiable manner on such parameters, primarily due to the physics of sudden interparticulate impact and transient dynamics associated with particulate flow. Clearly, these characteristics of Π make it difficult to treat with a classical gradient-based method, such as the quasi-Newton family of search methods. However, these difficulties can be mitigated by first employing non-derivative global-search schemes, such as simulated annealing, random search or genetic algorithms [89]. In particular, the author has developed robust genetic algorithms for inverse problems for various other models involving particulates, for example in References [52–54, 90]. Afterwards, gradient-based methods can be useful for enhancing, essentially post-processing, solutions found with a genetic algorithm, if the objective function is sufficiently smooth in that region of the parameter space.

REFERENCES

1. Benz W. From dust to planets. *Spatium* 2000; **6**:3–14.
2. Benz W. Impact simulations with fracture. 1. Method and tests. *Icarus* 1994; **107**:98–116.
3. Blum J, Wurm G. Impact simulations on sticking, restructuring, and fragmentation of preplanetary dust aggregates. *Icarus* 2000; **143**:138–146.
4. Dominik C, Tielens AGGM. The physics of dust coagulation and the structure of dust aggregates in space. *The Astrophysical Journal* 1997; **480**:647–673.
5. Chokshi A, Tielens AGGM, Hollenbach D. Dust coagulation. *The Astrophysical Journal* 1993; **407**:806–819.

6. Wurm G, Blum J, Colwell JE. A new mechanism relevant to the formation of planetesimals in the solar nebula. *Icarus* 2001; **151**:318–321.
7. Du Y, Li H, Kadanoff LP. Breakdown of hydrodynamics in a one-dimensional system of inelastic particles. *Physical Review Letters* 1995; **74**:1268.
8. Kokubo E, Ida S. Formation of protoplanets from planetesimals in the solar nebula. *Icarus* 2000; **143**(1): 15–270.
9. Kokubo E, Ida S. On runaway growth of planetesimals. *Icarus* 1996; **123**(1):180–191.
10. Mitchell P, Frenklach M. Particle aggregation with simultaneous surface growth. *Physical Review E* 2003; **67**:061407.
11. Grazier KR, Newman WI, Kaula WM, Hyman JM. Dynamical evolution of planetesimals in the outer solar system I. The jupiter/saturn zone. *Icarus* 2000; **140**(2):341–352.
12. Grazier KR, Newman WI, Varadi F, Kaula WM, Hyman JM. Dynamical evolution of planetesimals in the outer solar system II. The saturn/uranus and uranus/neptune zones. *Icarus* 1999; **140**(2):353–368.
13. Supulver KD, Lin DNC. Formation of icy planetesimals in a turbulent solar nebula. *Icarus* 2000; **146**(2): 525–540.
14. Tanga P, Babiano A, Dubrulle B, Provenzale A. Forming planetesimals in vortices. *Icarus* 1996; **121**(1): 158–170.
15. Cuzzi CN, Dobrovolskis AR, Champney JM. Particle-gas dynamics in the midplane of a protoplanetary nebula. *Icarus* 1993; **106**:102–134.
16. Weidenschilling SJ, Cuzzi JN. Formation of planetesimals in the solar nebula. *Protostars and Planets III*, Levy EH, Lunine JI (eds). University of Arizona Press: Tucson, 1993; 1031–1060.
17. Weidenschilling SJ, Spaute D, Davis DR, Marzari F, Ohtsuki K. Accretional evolution of a planetesimal swarm. *Icarus* 1997; **128**(2):429–455.
18. Beckwith S, Henning T, Nakagawa Y. Dust particles in protoplanetary disks. In *Protostars and Planets IVs*, Mannings V, Boss AP, Russell SS (eds). University of Arizona Press: Tuscon, 2000.
19. Barge P, Sommeria J. Did planet formation begin inside persistent gaseous vortices? *A&A*, L1-4, 1995.
20. Pollack JN, Hollenbach D, Beckwith S, Simonelli DP, Roush T, Fong W. Composition and radiative properties in molecular clouds and accretion disks. *The Astrophysical Journal* 1994; **421**:615–639.
21. Lissauer JJ. Planet formation. *Annual Review of Astronomy and Astrophysics* 1993; **31**:129–174.
22. Barranco J, Marcus P, Umurhan O. Scaling and asymptotics of coherent vortices in protoplanetary disks. In *Studying Turbulence Using Numerical Simulation. Databases-VIII*, *Proceedings of the Summer Program*, Center for Turbulence Research, Stanford University Press: Palo Alto, 2001.
23. Barranco J, Marcus P. Vortices in protoplanetary disks and the formation of planetesimals. In *Studying Turbulence Using Numerical Simulation. Databases-VIII*, *Proceedings of the Summer Program*, Center for Turbulence Research, Stanford University Press: Palo Alto, 2001.
24. Behringer RP. The dynamics of flowing sand. *Nonlinear Science Today* 1993; **3**:1.
25. Behringer RP, Baxter GW. Pattern formation, complexity and time-dependence in granular flows. *Granular Matter—An Interdisciplinary Approach*, Mehta A (ed.). Springer: New York, 1993; 85–119.
26. Behringer RP, Miller BJ. Stress fluctuations for sheared 3D granular materials. *Proceedings*, *Powders and Grains 97*, Behringer R, Jenkins J (eds). Balkema: Rotterdam, 1997; 333–336.
27. Behringer RP, Howell D, Veje C. Fluctuations in granular flows. *Chaos* 1999; **9**:559–572.
28. Tai Y-C, Noelle S, Gray JMNT, Hutter K. Shock capturing and front tracking methods for granular avalanches. *Journal of Computational Physics* 2002; **175**:269–301.
29. Tai Y-C, Gray JMNT, Hutter K, Noelle S. Flow of dense avalanches past obstructions. *Annals of Glaciology* 2001; **32**:281–284.
30. Tai Y-C, Noelle S, Gray JMNT, Hutter K. An accurate shock-capturing finite-difference method to slove the Savage–Hutter equations in avalanche dynamics. *Annals of Glaciology* 2001; **32**:263–267.
31. Gray JMNT, Wieland M, Hutter K. Gravity-driven free surface flow of granular avalanches over complex basal topography. *Proceedings of the Royal Society London*, *A* 1999; **455**:1841–1874.
32. Wieland M, Gray JMNT, Hutter K. Channelized free-surface flow of cohesionless granular avalanches in a chute with shallow lateral curvature. *Journal of Fluid Mechanics* 1999; **392**:73–100.
33. Berezin YA, Hutter K, Spodareva LA. Stability properties of shallow granular flows. *International Journal of Nonlinear Mechanics* 1998; **33**(4):647–658.
34. Gray JMNT, Hutter K. Pattern formation in granular avalanches. *Continuum Mechanics and Thermodynamics* 1997; **9**:341–345.

35. Gray JMNT. Granular flow in partially filled slowly rotating drums. *Journal of Fluid Mechanics* 2001; **441**:1–29.
36. Hutter K. Avalanche dynamics. In *Hydrology of Disasters*, Singh VP (ed.). Kluwer Academic Publishers: Dordrecht, 1996; 317–394.
37. Hutter K, Koch T, Plüss C, Savage SB. The dynamics of avalanches of granular materials from initiation to runout. Part II. Experiments. *Acta Mechanica* 1995; **109**:127–165.
38. Hutter K, Rajagopal KR. On flows of granular materials. *Continuum Mechanics and Thermodynamics* 1994; **6**:81–139.
39. Koch T, Greve R, Hutter K. Unconfined flow of granular avalanches along a partly curved surface. II. Experiments and numerical computations. *Proceedings of the Royal Society London*, *A* 1994; **445**:415–435.
40. Greve R, Hutter K. Motion of a granular avalanche in a convex and concave curved chute: experiments and theoretical predictions. *Philosophical Transactions of the Royal Society London A* 1993; **342**:573–600.
41. Hutter K, Siegel M, Savage SB, Nohguchi Y. Two-dimensional spreading of a granular avalanche down an inclined plane. Part I: theory. *Acta Mechanica* 1993; **100**:37–68.
42. Jaeger HM, Nagel SR. La Physique de l'Etat Granulaire. *La Recherche* 1992; **249**:1380.
43. Jaeger HM, Nagel SR. Physics of the granular state. *Science* 1992; **255**:1523.
44. Nagel SR. Instabilities in a sandpile. *Review of Modern Physics* 1992; **64**:321.
45. Liu CH, Jaeger HM, Nagel SR. Finite size effects in a sandpile. *Physical Review A* 1991; **43**:7091.
46. Liu CH, Nagel SR. Sound in a granular material: disorder and nonlinearity. *Physical Review B* 1993; **48**:15646.
47. Jaeger HM, Nagel SR. La Fisica del Estado Granular. *Mundo Cientifico* 1993; **132**:108.
48. Jaeger HM, Knight JB, Liu CH, Nagel SR. What is shaking in the sand box? *Material Research Society Bulletin* 1994; **19**:25.
49. Jaeger HM, Nagel SR, Behringer RP. The physics of granular materials. *Physics Today* 1996; **4**:32.
50. Jaeger HM, Nagel SR, Behringer RP. Granular solids, liquids and gases. *Reviews of Modern Physics* 1996; **68**:1259.
51. Jaeger HM, Nagel SR. Dynamics of granular material. *American Scientist* 1997; **85**:540.
52. Zohdi TI. Modeling and direct simulation of near-field granular flows. *The International Journal of Solids and Structures*, in press.
53. Zohdi TI. A computational framework for agglomeration in thermo-chemically reacting granular flows. *Proceedings of the Royal Society*, in press.
54. Zohdi TI. Computational design of swarms. *International Journal for Numerical Methods in Engineering* 2003; **57**:2205–2219.
55. Hale J, Kocak H. *Dynamics and Bifurcations*. Springer: Berlin, 1991.
56. Tabor D. Interaction between surfaces: adhesion and friction. In *Surface Physics of Materials*, vol. II, Chapter 10, Blakely JM (ed.). Academic Press: New York, San Francisco, London, 1975.
57. Haile JM. *Molecular Dynamics Simulations*: *Elementary Methods*. Wiley: New York, 1992.
58. Hase WL. *Molecular Dynamics of Clusters*, *Surfaces*, *Liquids*, and *Interfaces*. *Advances in Classical Trajectory Methods*, vol. 4. JAI Press: Greenwich, 1999.
59. Schlick T. *Molecular Modeling and Simulation: An Interdisciplinary Guide*. Springer: New York, 2000.
60. Rapaport DC. *The Art of Molecular Dynamics Simulation*. Cambridge University Press: Cambridge, 1995.
61. Moelwyn-Hughes EA. *Physical Chemistry*. Pergamon: Oxford, 1961.
62. Stillinger FH, Weber TA. Computer simulation of local order in condensed phases of silicon. *Physical Review B* 1985; **31**:5262–5271.
63. Tersoff J. Empirical interatomic potential for carbon, with applications to amorphous carbon. *Physical Review Letters* 1988; **61**:2879–2882.
64. Frenklach M, Carmer CS. Molecular dynamics using combined quantum and empirical forces: application to surface reactions. *Advances in Classical Trajectory Methods* 1999; **4**:27–63.
65. Johnson K. *Contact Mechanics*. Cambridge University Press: Cambridge, 1985.
66. Oden JT, Pires E. Nonlocal and nonlinear friction laws and variational principles for contact problems in elasticity. *ASME Journal of Applied Mechanics* 1983; **50**:67–76.
67. Martins JAC, Oden JT. Existence and uniqueness results in dynamics contact problems with nonlinear normal and friction interfaces. *Nonlinear Analysis* 1987; **11**:407–428.
68. Kikuchi N, Oden JT. *Contact Problems in Elasticity*: *A Study of Variational Inequalities and Finite Element Methods*. SIAM: Philadelphia, PA, 1988.

69. Klarbring A. Examples of nonuniqueness and nonexistence of solutions to quasistatic contact problems with friction. *Ingenieur-Archives* 1990; **60**:529–541.
70. Cho H, Barber JR. Stability of the three-dimensional Coloumb friction law. *Proceedings of the Royal Society* 1999; **455**(1983):839–862.
71. Wriggers P. *Computational Contact Mechanics*. Wiley: New York, 2002.
72. Goldsmith W. *Impact: The Theory and Physical Behavior of Colliding Solids*. Dover: Toronto, 2001 (Re-issue).
73. Schmidt L. *The Engineering of Chemical Reactions*. Oxford University Press: Oxford, 1998.
74. Bohren C, Huffman D. *Absorption and Scattering of Light by Small Particles*. Wiley Science Paperback Series. John Wiley: Chichester, 1998.
75. Zohdi TI. An adaptive-recursive staggering strategy for simulating multifield coupled processes in microheterogeneous solids. *International Journal for Numerical Methods in Engineering* 2002; **53**: 1511–1532.
76. Zohdi TI. Modeling and simulation of a class of coupled thermochemo-mechanical processes in multiphase solids. *Computer Methods in Applied Mechanics and Engineering* 2004; **193**(6–8):679–699.
77. Schrefler BA. A partitioned solution procedure for geothermal reservoir analysis. *Communications in Applied Numerical Methods* 1985; **1**:53–56.
78. Zienkiewicz OC. Coupled problems and their numerical solution. In *Numerical Methods in Coupled Systems*, Lewis RW, Bettes P, Hinton E (eds). Wiley: Chichester, 1984; 35–58.
79. Lewis RW, Schrefler BA, Simoni L. Coupling versus uncoupling in soil consolidation. *International Journal for Numerical and Analytical Methods in Geomechanics* 1992; **15**:533–548.
80. Lewis RW, Schrefler BA. *The Finite Element Method in the Static and Dynamic Deformation and Consolidation of Porous Media* (2nd edn). Wiley Press: New York, 1998.
81. Park KC, Felippa CA. Partitioned analysis of coupled systems. In *Computational Methods for Transient Analysis*, Belytschko T, Hughes TJR (eds). North Holland: Amsterdam, 1983.
82. Piperno S. Explicit/implicit fluid/structure staggered procedures with a structural predictor and fluid subcycling for 2D inviscid aeroelastic simulations. *International Journal for Numerical Methods in Fluids* 1997; **25**: 1207–1226.
83. Le Tallec P, Mouro J. Fluid structure interaction with large structural displacements. *Computer Methods in Applied Mechanics and Engineering* 2001; **190**(24–25):3039–3097.
84. Doltsinis ISt. Coupled field problems–solution techniques for sequential and parallel processing. In *Solving Large-Scale Problems in Mechanics*, Papadrakakis M (ed.). John Wiley: Chichester, 1993.
85. Doltsinis ISt. Solution of coupled systems by distinct operators. *Engineering Computations* 1997; **14**:829–868.
86. Chung J, Grigoropoulos C, Greif R. Infrared thermal velocimetry in MEMS-based fluid devices. *Journal of Microelectromechanical Systems* 1999; **12**(3):365–371.
87. Shin Y, Chung J, Kladias N, Panides E, Domoto J, Grigoropoulos CP. Compressible flow of liquid in standing wave tube. *Journal of Fluid Mechanics* 2003; preprint, submitted.
88. Ashauer M, Glosch H, Hedrich F, Hey N, Sandmaier H, Lang W. Thermal flow sensor for liquids & gases. In *Proceedings of the ASME International Mechanical Engineering Congress and Exposition*, Anaheim, CA, 1998; 427–432.
89. Holland JH. *Adaptation in Natural and Artificial Systems*. University of Michigan Press: Ann Arbor, MI, 1975.
90. Zohdi TI. Genetic optimization of statistically uncertain microheterogeneous solids. *Philosophical Transactions of the Royal Society*: *Mathematical*, *Physical and Engineering Sciences* 2003; **361**(1806):1021–1043.

